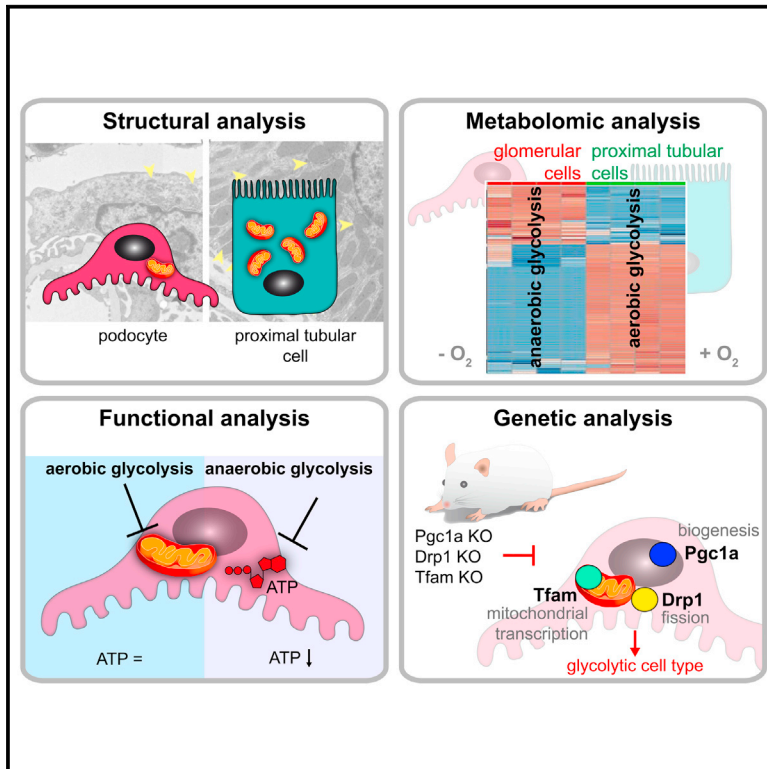


Anaerobic Glycolysis Maintains the Glomerular Filtration Barrier Independent of Mitochondrial Metabolism and Dynamics

Graphical Abstract



Authors

Paul T. Brinkkoetter, Tillmann Bork, Sarah Salou, ..., Christoph Handschin, Christoph Schell, Tobias B. Huber

Correspondence

t.huber@uke.de

In Brief

Glomerular podocytes form the third and most outer layer of the kidney filtration barrier responsible for restricting the passage of proteins into the urine. Brinkkoetter et al. show that podocyte metabolism primarily relies on anaerobic glycolysis and the fermentation of glucose to lactate.

Highlights

- Anaerobic glycolysis represents the predominant energy source of podocytes
- Neither mitochondrial turnover nor mtDNA transcription impairs podocyte function
- These findings elucidate podocyte metabolism, function, and glomerular integrity



Anaerobic Glycolysis Maintains the Glomerular Filtration Barrier Independent of Mitochondrial Metabolism and Dynamics

Paul T. Brinkkoetter,^{1,2,12} Tillmann Bork,^{3,12} Sarah Salou,^{3,12} Wei Liang,³ Athanasia Mizi,^{1,2} Cem Özel,^{1,2} Sybille Koehler,^{1,2} H. Henning Hagmann,^{1,2} Christina Ising,^{1,2} Alexander Kuczkowski,^{1,2} Svenia Schnyder,⁴ Ahmed Abed,³ Bernhard Schermer,^{1,2} Thomas Benzing,^{1,2} Oliver Kretz,⁵ Victor G. Puelles,^{5,10,11} Simon Lagies,^{6,7} Manuel Schlimpert,^{6,7} Bernd Kammerer,⁸ Christoph Handschin,⁴ Christoph Schell,⁹ and Tobias B. Huber^{5,13,*}

¹Department II of Internal Medicine and Center for Molecular Medicine Cologne (CMMC), University of Cologne, Faculty of Medicine and University Hospital Cologne, Cologne, Germany

²Cologne Cluster of Excellence on Cellular Stress Responses in Ageing-Associated Diseases (CECAD), Cologne, Germany

³Department of Medicine IV, Faculty of Medicine, University of Freiburg, Freiburg, Germany

⁴Biozentrum, University of Basel, Basel, Switzerland

⁵III. Department of Medicine, University Medical Center Hamburg-Eppendorf, Hamburg, Germany

⁶Spemann Graduate School of Biology and Medicine (SGBM), University of Freiburg, Freiburg, Germany

⁷Faculty of Biology, University of Freiburg, Freiburg, Germany

⁸BIOS Centre for Biological Signalling Studies, University of Freiburg, Freiburg, Germany

⁹Institute of Surgical Pathology, Faculty of Medicine, University of Freiburg, Freiburg, Germany

¹⁰Division of Nephrology and Clinical Immunology, University Hospital RWTH Aachen, Aachen, Germany

¹¹Department of Nephrology, Monash Health, Melbourne, VIC, Australia

¹²These authors contributed equally

¹³Lead Contact

*Correspondence: t.huber@uke.de

<https://doi.org/10.1016/j.celrep.2019.04.012>

SUMMARY

The cellular responses induced by mitochondrial dysfunction remain elusive. Intrigued by the lack of almost any glomerular phenotype in patients with profound renal ischemia, we comprehensively investigated the primary sources of energy of glomerular podocytes. Combining functional measurements of oxygen consumption rates, glomerular metabolite analysis, and determination of mitochondrial density of podocytes *in vivo*, we demonstrate that anaerobic glycolysis and fermentation of glucose to lactate represent the key energy source of podocytes. Under physiological conditions, we could detect neither a developmental nor late-onset pathological phenotype in podocytes with impaired mitochondrial biogenesis machinery, defective mitochondrial fusion-fission apparatus, or reduced mtDNA stability and transcription caused by podocyte-specific deletion of *Pgc-1 α* , *Drp1*, or *Tfam*, respectively. Anaerobic glycolysis represents the predominant metabolic pathway of podocytes. These findings offer a strategy to therapeutically interfere with the enhanced podocyte metabolism in various progressive kidney diseases, such as diabetic nephropathy or focal segmental glomerulosclerosis (FSGS).

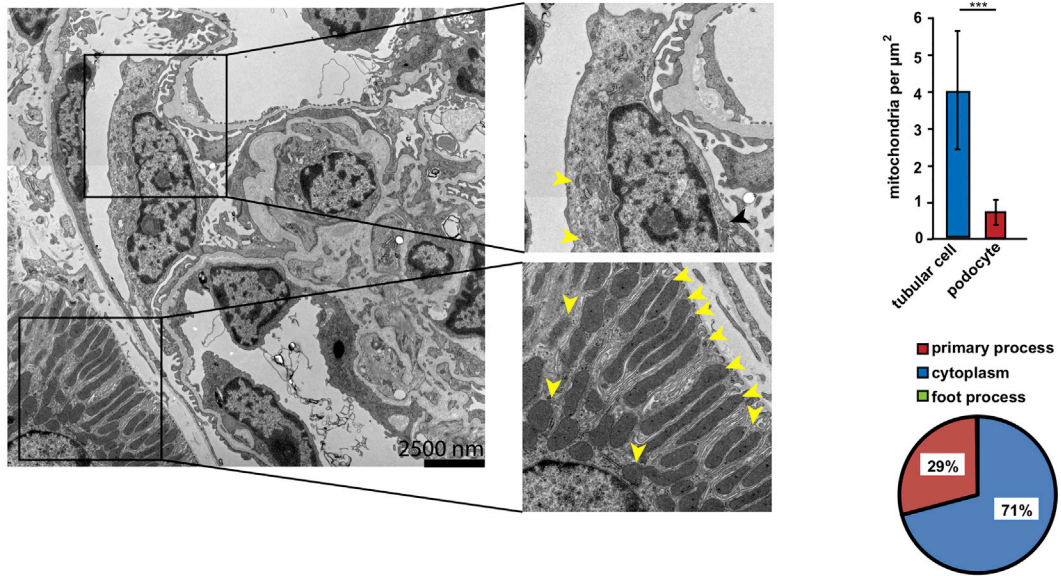
INTRODUCTION

Mitochondria are key organelles for cellular bioenergetics and constantly undergo dynamic remodeling processes, including fusion and fission to adjust to the cellular demand for energy. Mitochondrial dysfunction, impaired energy homeostasis, as well as an increased production of reactive oxygen species are associated to a variety of human disorders, including aging-associated diseases (Bratic and Larsson, 2013; Nunnari and Suomalainen, 2012) as well as kidney diseases (reviewed in O'Toole, 2014). The contribution of mitochondrial dysfunction to disease onset or progression—either directly due to genetic mutations or indirectly as a consequence of an altered cellular homeostasis—remains unclear, especially in complex multi-causal disorders, such as diabetic nephropathy, the leading cause of end-stage renal disease (ESRD) in western countries. Therefore, understanding the functional role of mitochondria in the two essential compartments of the kidney, i.e., glomerulus and tubular system, is a crucial first step.

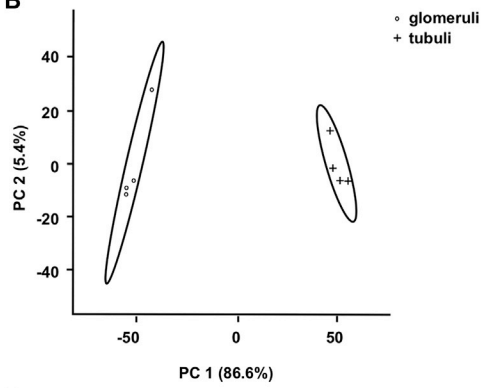
Mitochondria are the primary cellular source of ATP and essential for all eukaryotic cells (Detmer and Chan, 2007). They are highly dynamic structures that constantly divide and fuse to build an intracellular network that assures the distribution within the cell and is required to execute their pleiotropic activities, including among others aerobic ATP production, governing metabolic pathways, as well as apoptosis, participation in RNA and DNA production, and the biosynthesis of heme, certain amino acids, and lipids (Ising et al., 2015; Osman et al., 2011; Schmidt et al., 2010). In addition, the inner mitochondrial



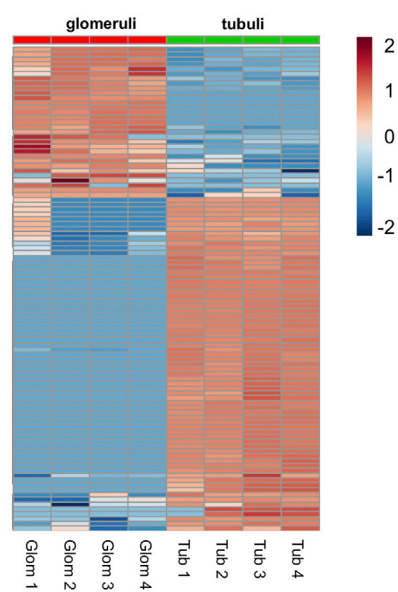
A



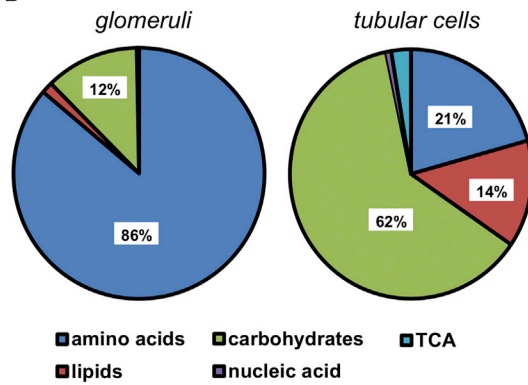
B



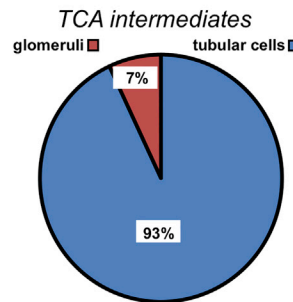
C



D



E



(legend on next page)

membrane potential participates in the uptake of cytosolic Ca^{2+} and potentially serves as buffer for locally increased intracellular Ca^{2+} levels (von Kleist-Retzow et al., 2007). To this end, mitochondria maintained their ability for self-replication to face the metabolic energy demands of the cell. Adaptive mechanisms of the mitochondrial network operating energy metabolism and mitochondrial self-renewal are mitochondrial biogenesis and mitochondrial dynamics regulated by key molecules, including mitochondrial transcription factor A (TFAM), peroxisome proliferator-activated receptor gamma coactivator 1-alpha (PGC-1 α), and dynamin-related protein 1 (DRP-1).

Primary mitochondrialopathies mainly affect the CNS and skeletal muscle. In most cases, the renal involvement is limited to tubular dysfunction, comprising Fanconi or Bartter-like syndromes or renal tubular acidosis (reviewed in Che et al., 2014), reflecting the high ATP demand derived from mitochondrial OXPHOS necessary for electrolyte-transporting processes within the tubular apparatus. Only sporadically, mitochondrialopathies are also linked to glomerular disease, in particular focal segmental glomerulosclerosis (FSGS) and steroid-resistant nephrotic syndrome (reviewed in O'Toole, 2014). Moreover, another highly relevant clinical condition, i.e., acute kidney injury (AKI), emphasizes a different role of mitochondria in the two kidney compartments. AKI due to ischemia and reperfusion injury causes severe tubular dysfunction and, eventually, tubular necrosis and necroptosis (reviewed in Kers et al., 2016), whereas the glomerular compartment remains functionally and morphologically intact. These findings cannot be simply explained by general differences in the cellular energy demand. As tubular function can be characterized as a highly energy-consuming process, so does the maintenance of the structural integrity of the glomerular filter.

The majority of kidney diseases evolve from the glomerulus, the renal filtration unit. The glomerular filter is composed of three anatomic layers: the fenestrated endothelial cell layer; the glomerular basement membrane (GBM); and the slit diaphragm between adjacent podocyte foot processes. Podocytes are pericyte-like epithelial cells that cover the outer aspect of the glomerular capillaries (reviewed in Brinkkoetter et al., 2013). The cells have to apply static forces to cope with the pulsating glomerular capillaries to maintain the glomerular filtration barrier. These include adaptive processes comprising actin-based cytoskeletal remodeling and hypertrophy to adjust for filtration demands. The critical function of these processes has been demonstrated in various podocyte-specific knockout approaches targeting hypertrophy and actin remodeling (Gödel et al., 2011; Schell et al., 2013; Zschiedrich et al., 2017), all leading to a uniform pathological sequel involving foot process

effacement and detachment, and proteinuria is the most sensitive clinical parameter reflecting podocyte damage (de Jong and Curhan, 2006; Pinto-Sietsma et al., 2000).

In order to sustain the complex cellular morphology of interdigitating foot processes, podocytes rely on a constant energy supply and reservoir. It is so far not yet clear what kind of energy resources and pathways are mainly exploited under physiological conditions (Abe et al., 2010; Müller-Deile and Schiffer, 2014). Moreover, there are conflicting results in glomerular disease concerning the role of mitochondria (Doleris et al., 2000; Hotta et al., 2001; Imasawa and Rossignol, 2013; Kurogouchi et al., 1998; Yamagata et al., 2002), suggesting an unmet need to delineate the bioenergetic framework required to maintain the glomerular filter under physiological conditions and characterize the role of mitochondria in this unique functional compartment. Here, we applied an unbiased metabolomic approach to determine the podocytes' energy supply chain with special emphasis on the contribution of mitochondria. Therefore, we employed conditional *in vivo* targeting strategies specifically in podocytes to interfere with mitochondrial biogenesis by depleting *PPARGC1A* (later referred to as *Pgc-1 α*), to inhibit mitochondrial fission by depleting *DNM1L* (later referred to as *Drp1*), and to diminish mtDNA copy number and transcription by deleting *Tfam*.

RESULTS

Podocytes Display Low Mitochondrial Density

First, we performed transmission electron microscopy (TEM) to study the mitochondrial abundance and localization within glomerular podocytes. To this end, we analyzed 70 TEM pictures from 8 wild-type mice (Figure 1A). Podocytes showed a significantly lower mitochondrial density per cell area as compared to renal tubular cells (0.7 ± 0.7 versus 4.1 ± 1.6 ; $p \leq 0.001$). Moreover, in podocytes, mitochondria were primarily found within the cytoplasm (71%) and primary processes (29%) but rarely seen within secondary processes. 3D-reconstructed glomeruli stained for the mitochondrial enzyme SOD2 (superoxide dismutase 2) and the glycolytic enzyme PKM2 (pyruvate kinase M2) confirmed the perinuclear localization of mitochondria (Figure S1A), whereas PKM2 was found ubiquitously, suggesting podocyte processes as a large putative compartment of anaerobic glycolysis (Figures S1B–S1D). Principal-component analysis (PCA) of metabolite content of glomeruli and the tubular compartment (obtained from 4 mice each) revealed a distinct metabolite pattern (Figures 1B and 1C), with high levels of amino acids (86%) and low levels of carbohydrates (12%) and lipids (1.4%) in glomeruli, although in the tubular compartment,

Figure 1. Podocytes Display Low Mitochondrial Density

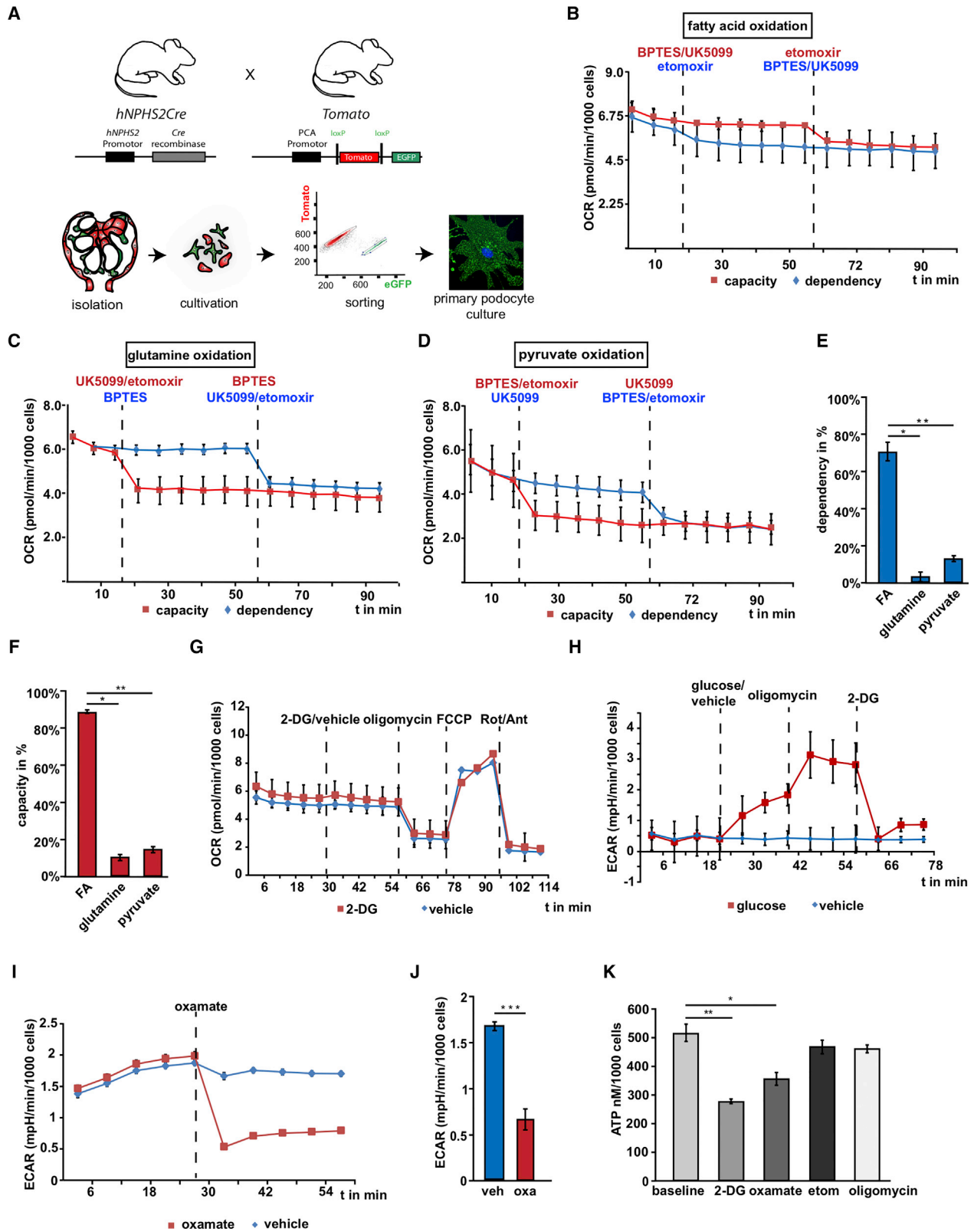
(A) Image obtained by transmission electron microscopy (TEM) displaying a glomerulus with neighboring tubular cells. Boxed areas show details from a podocyte and a proximal tubular cell, respectively. Mitochondria are marked by arrowheads. The depicted image is stitched from a 3×3 array of single images. Quantification of mitochondrial density and distribution of mitochondria in podocytes (based on the analysis of 70 pictures obtained from 8 mice; *** $p \leq 0.001$; presented as mean \pm SD).

(B) Principal-component analysis (PCA) of metabolite content of glomeruli and the tubular compartment (obtained from 4 mice each).

(C) Heatmap of metabolites detected in glomeruli and in the tubular compartment (obtained from 4 mice each).

(D) Metabolite composition of glomerular and tubular samples based on superclasses of metabolites.

(E) Abundance of intermediates of tricarboxylic acid (TCA) cycle in glomeruli and the tubular compartment.



(legend on next page)

carbohydrates were most abundant (carbohydrates 62%, amino acids 21%, and lipids 14%; [Figure 1D](#)). These observations of fundamental metabolic differences were also reflected by low levels of intermediates of the tricarboxylic acid cycle (TCA) found in glomeruli compared to the tubular compartment (7% versus 93%; [Figure 1E](#)).

Glycolysis and oxidative phosphorylation (OXPHOS) are the two major cellular pathways to produce energy. Most cells may switch between these pathways in order to cope with changing energy demands. Glycolysis reflects the conversion of glucose into pyruvate and, subsequently, into lactate in the cytoplasm (anaerobic glycolysis) or into CO₂ and H₂O within mitochondria (aerobic glycolysis). In addition, mitochondrial energy may also be derived from oxidation of fatty acids and glutamine. The podocytes' mitochondrial dependency on and flexibility for each of these energy sources can be determined by measuring the decline in oxygen consumption rate (OCR) upon addition of specific inhibitors (dependency % = [baseline OCR – target inhibitor OCR/baseline OCR – all inhibitors OCR] × 100; capacity % = (1 – [baseline OCR – other 2 inhibitors OCR]/[baseline OCR – all inhibitors OCR]) × 100). To gain further insights in the podocytes' energy sources under physiological conditions, we isolated primary podocytes from wild-type reporter mice ([Figure 2A](#)). First, we analyzed the mitochondrial contribution to the energy supply chain. Administration of etomoxir, an inhibitor of long fatty acid oxidation, resulted in a significant decrease in OCR, and inhibition of glutamine (by bis-2-(5-phenylacetamido-1,3,4-thiadiazol-2-yl)ethyl sulfide [BPTES]) or pyruvate (by UK5099) oxidation resulted in marginal reductions of OCR only ([Figures 2B–2D](#)). These findings revealed that podocytes primarily utilize fatty acid oxidation and oxidation of glutamine or pyruvate is of minor importance ([Figures 2C–2F](#)). Next, we aimed to differentiate the podocytes' dependency on the anaerobic glycolysis and the activity of the respiratory chain. To this end, we measured the OCR of primary podocytes after administration of 2-deoxyglucose (2-DG), a glycolysis inhibitor competitively inhibiting the production of glucose-6-phosphate or vehicle followed by specific inhibitors (oligomycin, carbonyl cyanide-4-(trifluoromethoxy)phenylhydrazone [FCCP], and rotenone/antimycin A) of the respiratory chain ([Figure 2G](#)). The

administration of 2-DG did not affect the OCR neither at baseline nor after addition of the OXPHOS inhibitors. We also measured the extracellular acidification rate (ECAR) to determine the release of protons into the supernatant as a result of the activity of the glycolysis pathway ([Figure 2H](#)). Podocytes showed a rapid glucose-induced increase in glycolytic activity with a maximal glycolytic capacity of 3.1 ± 0.5 mpH/min/1,000 cells after inhibition of the mitochondrial ATP production by addition of oligomycin. These findings were further substantiated by assessing the oxamate-sensitive ECAR rate ([Figures 2I and 2J](#)), confirming the observation that podocytes harbor a strong glycolytic activity. Last, we assessed the contribution of the distinct ATP-generating pathways to the overall ATP production in podocytes ([Figure 2K](#)). Although inhibition of the anaerobic glycolysis by administration of 2-DG or oxamate resulted in a significant decrease in the cellular ATP content, inhibition of O₂-dependent pathways, including fatty acid oxidation, was of minor relevance. Taken together, low mitochondrial abundance, decreased levels of TCA intermediates, as well as a strong dependency on the anaerobic glycolysis support the hypothesis that podocytes do not primarily rely on mitochondrial energy resources under physiological conditions. To further substantiate this hypothesis, we explored phenotypes in three independent mouse models to interfere with mitochondrial function within podocytes specifically.

Podocytes Do Not Rely on Functional Mitochondrial Fission Machinery

First, we evaluated the structural and functional consequences of a targeted deletion of *Drp1* and the inability to undergo mitochondrial fission in podocytes. We monitored knockout and respective wild-type animals for a period of 12 months. Within this time period, we did not observe significant differences in body weight gain or any increase in urinary albumin excretion, excluding podocyte dysfunction in *Drp1* podocyte knockout animals ([Figure 3](#)). Histological evaluation revealed no obvious morphological alterations up to 12 months of age ([Figure 3H](#)). Using TEM, we visualized the mitochondrial morphology in podocytes of 1-, 5-, and 7-month-old *Drp1^{fllox/fllox}hNPHS2Cre* knockout and *Drp1^{fllox/fllox}* control mice. Although mitochondria

Figure 2. Primary Podocytes Rely on Glycolysis

(A) Primary podocyte culture was obtained by crossing *hNPHS2Cre* mice with a *Tomato/EGFP* reporter strain. Schematic of glomerular culture followed by fluorescence-activated cell sorting (FACS) is shown.

(B) Dependency and capacity of fatty acid oxidation obtained after etomoxir and BPTESm UK5099 injection or BPTES, UK5099 followed by etomoxir, respectively (mean ± SD). Final concentrations: etomoxir: 100 μM; BPTES: 30 μM; UK5099: 30 μM.

(C) Dependency and capacity of glutamine oxidation obtained after BPTES and etomoxir, UK5099 or etomoxir, UK5099 followed by BPTES, respectively (mean ± SD). Final concentrations: etomoxir: 100 μM; BPTES: 30 μM; UK5099: 30 μM.

(D) Dependency and capacity of pyruvate oxidation obtained after UK5099 and etomoxir, BPTES and etomoxir, BPTES followed by UK5099, respectively (mean ± SD). Final concentrations: etomoxir: 100 μM; BPTES: 30 μM; UK5099: 30 μM.

(E) Statistics displaying substrate dependency of primary podocytes (data out of 3 experiments; *p ≤ 0.05; **p ≤ 0.01; mean ± SD).

(F) Statistics displaying substrate capacity of primary podocytes (data out of 3 experiments; *p ≤ 0.05; **p ≤ 0.01; mean ± SD).

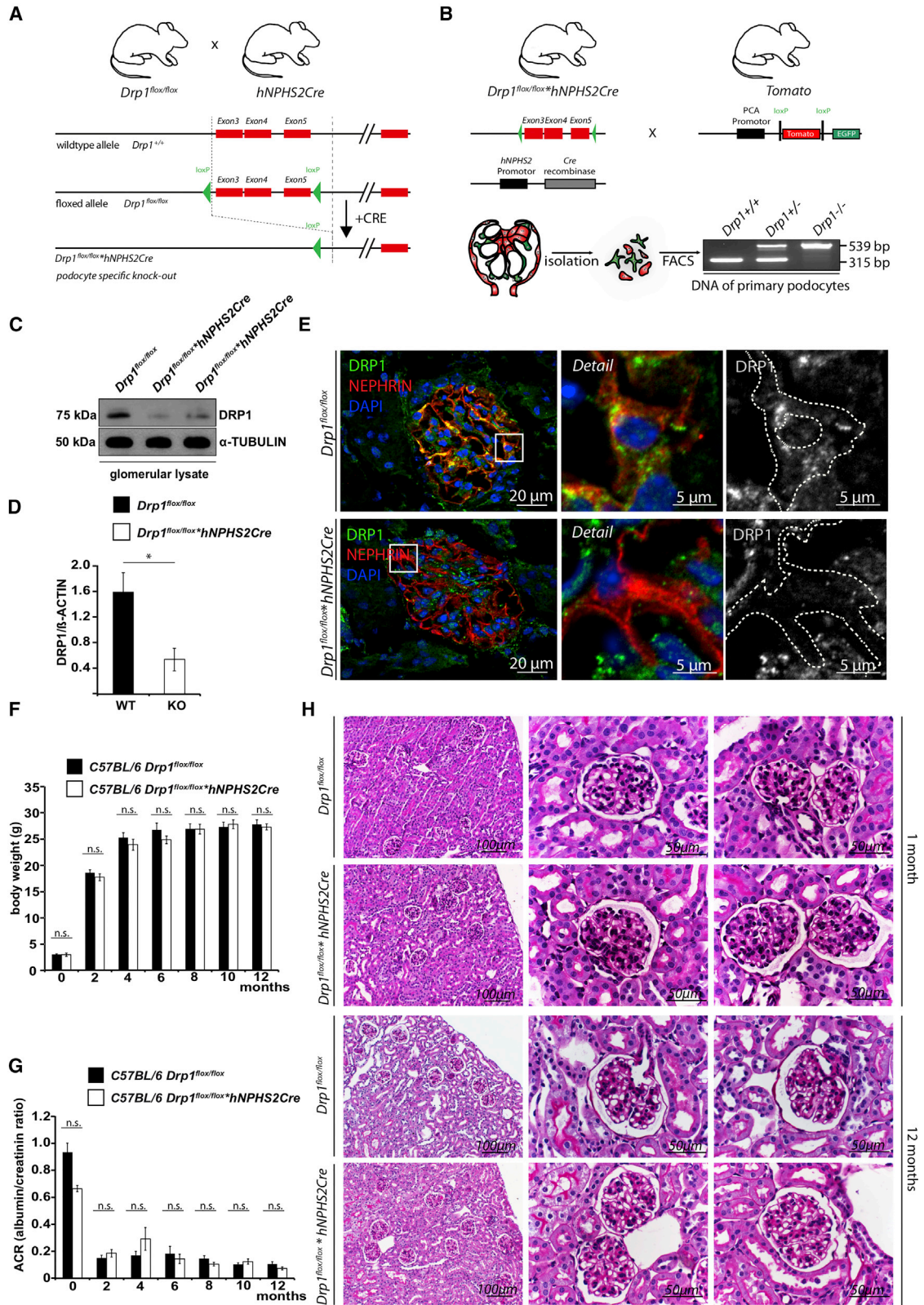
(G) Oxygen consumption rate (OCR) of primary podocytes after injection of 2-deoxyglucose or vehicle followed by the inhibitors of the respiratory chain as indicated (mean ± SD). Final concentration: 2-DG: 50 mM; oligomycin: 1 μM; FCCP: 0.5 μM; rotenone: 0.5 μM; antimycin: 0.5 μM.

(H) Extracellular acidification rate (ECAR) of primary podocytes obtained after injection of glucose or vehicle followed by oligomycin and 2-DG as indicated (mean ± SD). Final concentration: 2-DG: 50 mM; oligomycin: 1 μM; rotenone: 0.5 μM; antimycin: 0.5 μM.

(I) ECAR of primary podocytes after oxamate or vehicle injection (mean ± SD). Final concentration: oxamate: 45 mM.

(J) Statistics displaying ECAR after vehicle or oxamate injection (**p ≤ 0.001; mean ± SD).

(K) Statistics showing intracellular ATP content after 24-h treatment with 2-DG, oxamate, etomoxir, or oligomycin (*p ≤ 0.05; **p ≤ 0.01; mean ± SD). Final concentration: 2-DG: 50 mM; oxamate: 45 mM; etomoxir: 100 μM; oligomycin: 1 μM.



(legend on next page)

in podocytes of 1-month-old knockout mice seemed to form a more distinctive tubular network, no other major abnormalities were detected (Figures 4A and 4B). At months 5 and 7, mitochondria of *Drp1* knockout mice appeared slightly swollen, probably reflecting the consequences of deficient mitochondrial division and accumulation of oxidative stress. However, even at these later time points, no signs of podocyte foot process effacement were detectable in *Drp1* knockout mice (Figures 4C–4F).

To further delineate the function of *Drp1* on podocyte metabolism, *in vivo* and *in vitro* mtDNA levels were quantified in isolated glomeruli obtained from 24-week-old mice with podocyte-specific deletion of *Drp1* and respective controls as a surrogate parameter of mitochondrial density. mtDNA was significantly reduced in mice lacking DRP1, as highlighted by reduced *Atp6* and *Cox1* abundance compared to 18 s (Figure S2A). Functionally, gas chromatography-mass spectrometry (GC-MS) profiling from kidney cortex of respective mice revealed only minor differences on overall metabolite content and similar levels of lactate (Figure S2B). To further elucidate the potential impact of *Drp1* depletion on podocyte metabolism, small interfering RNA (siRNA)-based knockdown approaches were performed with subsequent metabolic profiling. Using this approach, cellular DRP1 content significantly decreased (Figure S2C); however, mitochondrial function and glycolysis as well as glycolytic capacity remained unaffected (Figures S2D–S2G). Maximal respiratory capacity as assessed after FCCP exposure was even increased compared to siScrambled controls, suggesting a role of DRP1 in mitochondrial stress response (Figure S2E). Assessment of the main mitochondrial fuel confirmed fatty acids a key source of podocyte OXPHOS. Knockdown of *Drp1*, however, did not affect mitochondrial fuel preference (Figures S2H–S2O). In summary, *Drp1* deletion impacted the expression of certain mitochondria-encoded genes; however, further functional effects were not detectable.

Mitochondrial Biogenesis Is Dispensable for Podocyte Function

Next, we interfered with mitochondrial biogenesis and deleted *Pgc-1 α* in podocytes specifically. We monitored *Pgc-1 α* knockout and respective wild-type animals for a period of 22 months. Again, we did not observe any significant differences neither in body weight nor in urinary albumin excretion (Figure 5). Histological evaluation revealed no obvious morphological alter-

ations nor did we detect structural mitochondrial defects by TEM (Figures 5E and 5F). Ultrastructure of podocyte foot processes remained intact (Figure 5F). Functionally, *Pgc-1 α* deletion reduced the mtDNA content in mouse glomeruli with regard to *Atp6* levels, suggesting reduced mitochondrial biogenesis (Figure S3A). However, GC-MS profiling of kidney cortex of mice with podocyte-specific deletion of *Pgc-1 α* and respective controls revealed only minor changes in overall metabolite content. Accordingly, lactate levels did not differ between the genotypes (Figure S3B). Knockdown of *Pgc-1 α* in human podocytes significantly reduced mitochondrial function and increased glycolysis and glycolytic capacity (Figures S3C–S3G), thereby demonstrating the impact of *Pgc-1 α* on mitochondrial biogenesis in podocytes and anaerobic glycolysis as a “back up” pathway to cover podocyte’s energy demands. Depletion of PGC-1 α did not impact mitochondrial substrate preference, as seen by maintained high levels fatty acid dependency and capacity (Figures S3H–S3O).

Loss of Mitochondrial Transcription and Lack of the OXPHOS Machinery Does Not Result in Podocyte Disease

Furthermore, we studied podocyte-specific *Tfam* knockout mice in order to provide additional *in vivo* evidence and to test the hypothesis that podocytes do not rely on the mitochondrial OXPHOS machinery. We followed knockout and wild-type animals for a period of 12 months and assessed renal function and proteinuria. As shown for *Drp1* and *Pgc-1 α* podocyte-specific knockout mice, again, we did not observe any significant differences neither in body weight nor in urinary albumin excretion (Figure 6). Histological evaluation revealed no obvious morphological alterations (Figure 6H). Additional TEM studies in 20- and 55-week-old animals revealed a regular slit diaphragm structure (Figure S4A) and no major structural abnormalities in mitochondrial morphology or number (Figures S4B and S4C). However, *Tfam* depletion significantly reduced mtDNA content in *ex vivo* isolated glomeruli (Figure S5A) and showed the strongest impact on overall metabolite composition as seen in the principal-component analysis (Figure S5B) compared to the other knockout models. In particular, lactate levels significantly increased if TFAM is lacking. Transient knockdown of *Tfam* in human podocytes (as demonstrated in Figure S5C) significantly reduced mitochondrial respiration and respiratory capacity

Figure 3. Loss of DRP1 Does Not Affect Glomerular Function and Morphology

(A) Schematic illustrating targeted gene deletion approach of *Drp1* in podocytes using the Cre-loxP system.

(B) Breeding strategy to generate a podocyte-based reporter strain. After isolation of GFP+ podocytes via FACS, DNA was prepared and respective genotypes were verified using the following primers: D1 (5'-CACTGAGAGCTCTATATGTAGGC-3'); D3 (5'-ACCAAAGTAAGGAATAGCTGTTG-3'); and D5 (5'-GAGTACC TAAAGTGGACAAGAGGTCC-3'). PCR products were detected at 315 bp and 539 bp.

(C) Western blot analysis confirmed reduced DRP1 levels in glomeruli of conditional *Drp1^{fllox/fllox}hNPHS2Cre* mice.

(D) Densitometric quantification of DRP1 protein levels demonstrated a significant reduction in glomeruli derived from KO animals (n = 3; *p \leq 0.05; mean \pm SD).

(E) Immunofluorescence stainings visualized absence of DRP1 in knockout podocytes. Dotted lines indicate the respective podocyte compartment, as marked with NEPHRIN staining.

(F) 12-month follow-up period revealed no differences in body weight between wild-type and *Drp1* knockout animals (at least 3 animals per genotype and time point were analyzed; mean \pm SD).

(G) Measurement of ACR (albumin-to-creatinine ratio) revealed no differences during the 12-month follow-up period (at least 3 animals per genotype and time point were analyzed; mean \pm SD).

(H) Periodic acid Schiff (PAS)-stained kidney sections obtained from 1-month-old and 12-month-old *Drp1^{fllox/fllox}hNPHS2Cre* mice and littermate controls showed normal glomerular structure.

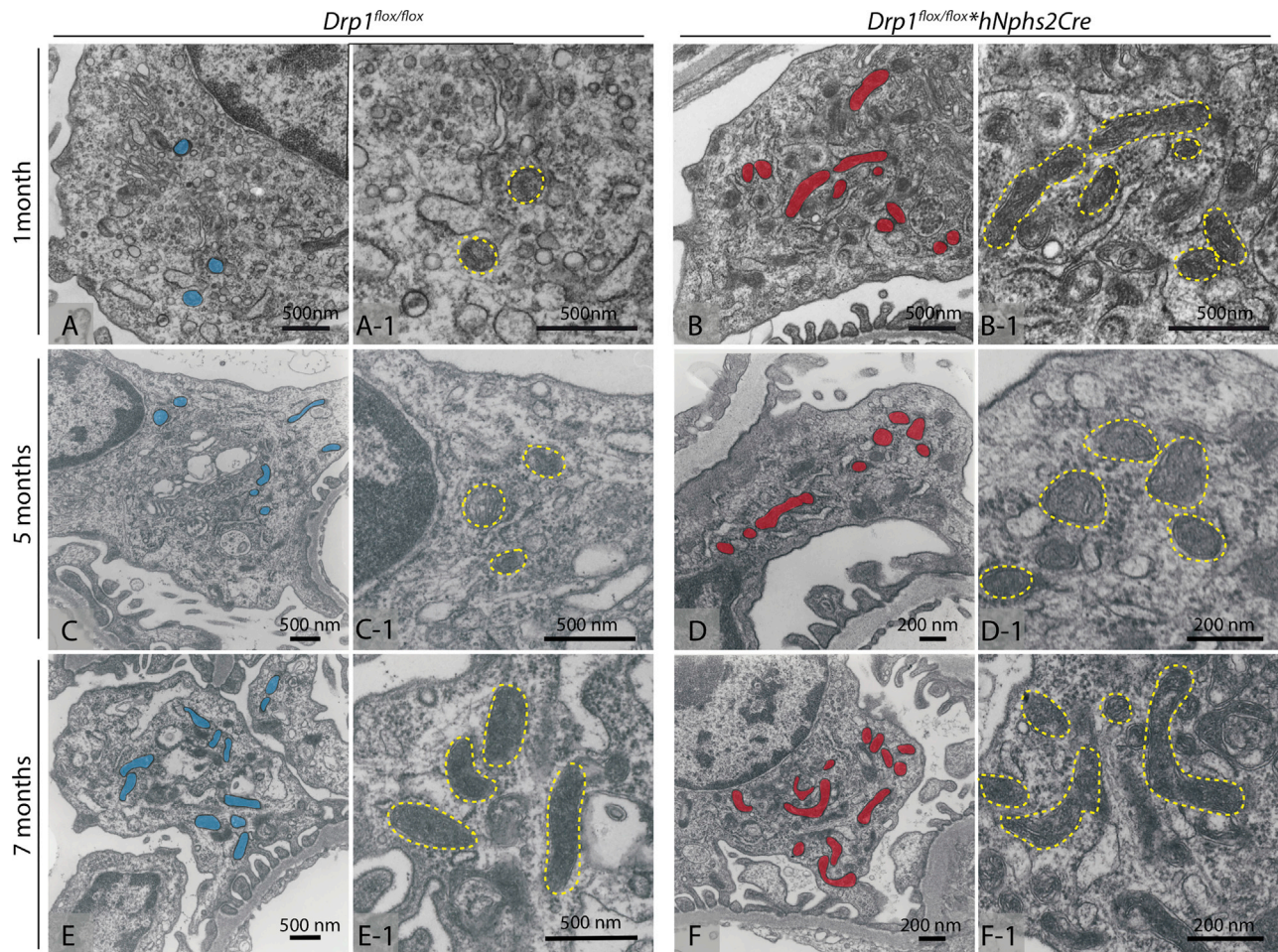


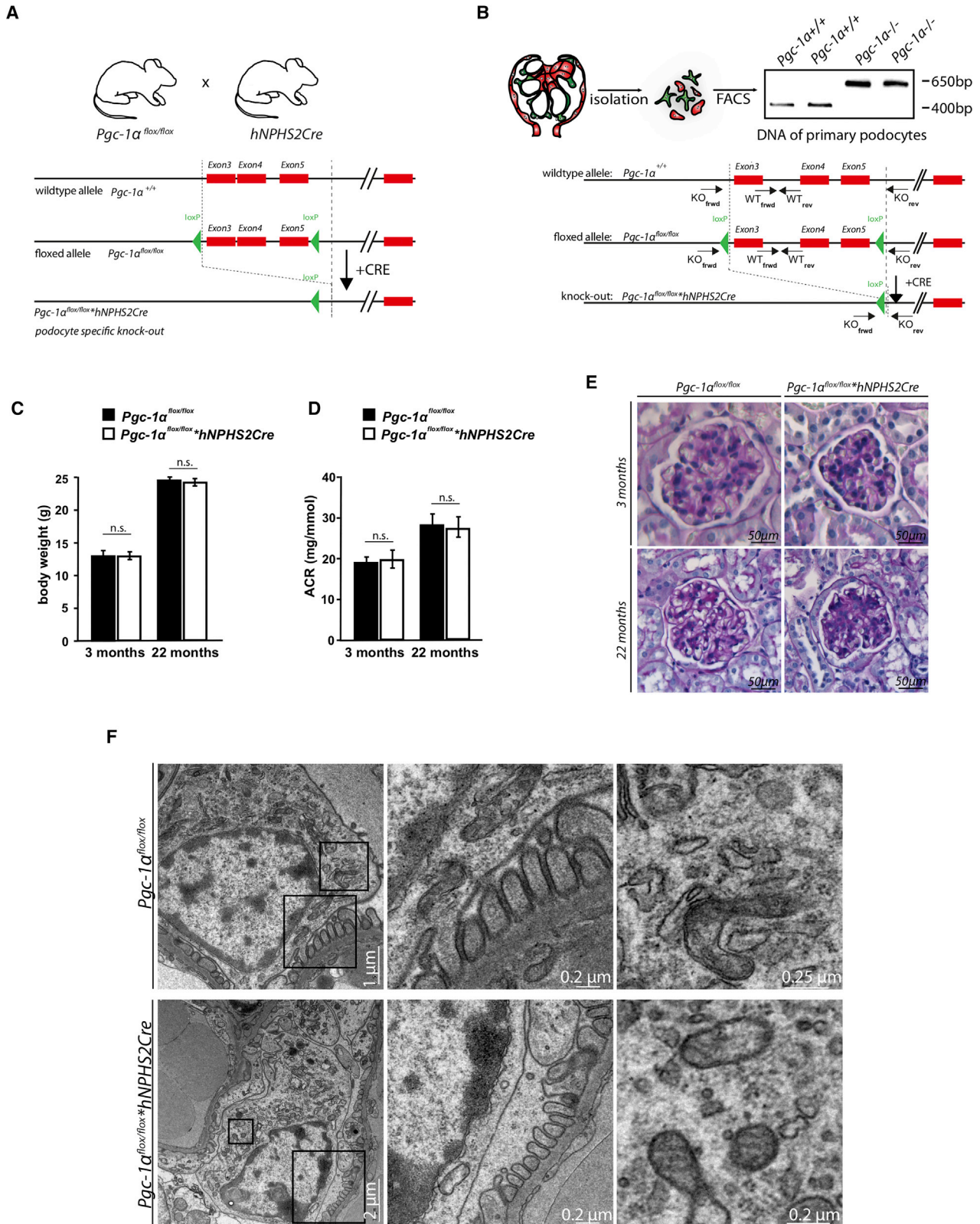
Figure 4. Mitochondria Are Elongated in *Drp1*-Deficient Podocytes

Representative TEM pictures displaying mitochondrial shape and density in podocytes. Sections were obtained from mouse kidneys at the age of 1 month, 5 months, and 7 months, respectively.

(Figures S5D and S5E). Glycolysis and glycolytic capacity significantly increased (Figures S5F and S5G). As seen in *Drp1* and *Pgc-1 α* knockdown experiments, fatty acids remain the main fuel for podocyte OXPHOS *in vitro* (Figures S5H–S5O).

Because knockdown of *Tfam* by using siRNA did not allow for complete abrogation of the protein, we aimed to further validate our findings by isolating primary podocytes after additional matings of *Tfam* podocyte knockout mice with a fluorescent reporter mouse (Figure 7A). Surprisingly, we did not observe any clear morphologic effect on the mitochondrial network (Figure 7B). However, as a result of the decrease in TFAM, we observed a differential regulation of proteins of the respiratory chain. Protein expression of mitochondrial-encoded genes, such as mtNdufb8, mtCO1, and ATP5A, were strongly decreased, reflecting an abrogated mitochondrial transcription and a strong reduction of complex I, IV, and V of the respiratory chain. The level of ubiquinol-cytochrome C reductase (UQCR) of complex III was only slightly reduced. By contrast, we did observe a strong reduction in the succinate dehydrogenase (ubiquinone) iron-sulfur subunit (SDHB) of complex II in the absence of TFAM, which is primarily

nuclear encoded (Figure 7C). OCR of *Tfam* knockout podocytes was strongly reduced, indicating severe abrogation of OXPHOS as intended (Figures 7D and 7E). Severe mitochondrial dysfunction was associated with strongly reduced reactive oxygen species (ROS) production as observed in *Tfam* knockout podocytes compared to wild-type (WT) and heterozygous *Tfam* deletion (Figure 7F). Surprisingly, anaerobic glycolysis and glycolytic capacity decreased as well *in vitro* (Figures 7G and 7H), however, still allowing for maintained podocyte ATP supply, as indicated by podocyte integrity *in vivo*. In summary, compared to the other knockout models in this study, deletion of *Tfam* showed the strongest impact on mitochondrial function and podocyte metabolism *in vivo* and *in vitro*. Neither *Drp1* nor *Pgc-1 α* or *Tfam* deletion was able to induce phenotypic abnormalities in podocytes *in vivo*. Accordingly, GC-MS profiling revealed only slight and distinct metabolic changes in *ex vivo* isolated kidney cortex of these mice (Figures S6A and S6B), suggesting a functionally fully compensated metabolic state due to increased anaerobic glycolysis in these models if mitochondria become genetically targeted.



(legend on next page)

DISCUSSION

Mitochondria are semi-autonomous organelles, the “cell’s power plants,” that produce the most of its ATP supply via the OXPHOS. Beyond energy supply, they are involved in crucial pathways for homeostasis, phagocytosis, and apoptosis. Mitochondria are also recognized as an important signaling platform that utilizes molecules like ADP and ATP, Ca^{2+} , respiratory chain metabolites, ROS, or the unfolded protein response to regulate cross-communication with other organelles and the nucleus (reviewed in Raimundo, 2014). Preservation and fitness of this crosstalk, under physiological or stress conditions, is necessary for normal cell function and homeostasis and alterations often result in pathological phenotypes. However, the regulatory mechanisms of this vital communication between the cell compartments in states of health and disease remain unclear. Mitochondrial genome regulation as well as the organelles distribution into the cell—specified by balanced fission and fusion—must be in accordance to tissue-dependent cellular needs. Respiratory activity of each tissue type determines the energetic threshold under which mitochondrial impairment leads to a disease phenotype. Although, so far, mitochondrial diseases were assigned to OXPHOS impairment, during the last years there are accumulating data supporting that impairment of mitochondria signaling can lead to disease independently of the energy production levels (Raimundo et al., 2012).

It is the matter of a long-standing debate to what extent the resident cells of the glomerulus, and in particular the podocytes, contribute actively to the filtering process. Glomeruli are thought to filter the plasma continuously, but filtration rates vary strongly dependent on physiological regulation, nephron type, and metabolic activity (Singer, 2001). There is, however, a general consensus that podocytes are essential for the buildup of the glomerular filtration barrier as they orchestrate glomerular endothelial cell functions through secreted vascular endothelial growth factor (VEGF; reviewed in Bartlett et al., 2016) and maintain the structural and functional integrity of the glomerular basement membrane (reviewed in Miner, 2012). Moreover, the fact that GBM and slit diaphragm component synthesis occurs in podocytes reveals their crucial role in maintaining the kidney filtration barrier, as well as their involvement in glomerular disease development. Podocytes represent the outer layer of the vascular filter counterbalancing mechanic forces as the result of a pulsatile blood flow. Hence, it is not surprising that podocytes harbor an actin-based cytoskeleton,

including a contractile machinery allowing rapid shape remodeling and podocyte movement (Peti-Peterdi and Sipos, 2010). Podocytes fine-structure and function maintenance implies metabolic activity, but so far their detailed metabolic profile remains obscure (reviewed in Imasawa and Rossignol, 2013). In 2010, Abe and colleagues provided first experimental evidence for a critical role of mitochondria and, in particular, a high dependency of podocytes on mitochondrial energy delivery using an immortalized podocyte cell line (Abe et al., 2010). Inhibition of glycolysis or oxidative phosphorylation each reduced ATP levels and were thought to explain the susceptibility of podocytes to oxidative stress as observed in patients with diabetic nephropathy. On the contrary, Ozawa et al. (2015) suggested that both glycolytic and OXPHOS pathways contribute to podocyte energy supplements, depending on the intracellular sub-localization of mitochondria and on the cell differentiation status. Imasawa et al. (2017) recorded that high-glucose conditions forced differentiating human podocyte cell lines to switch from OXPHOS to glycolysis, resulting in lactic acidosis. Here, we provide comprehensive metabolomics data from freshly isolated glomeruli and primary podocytes as well as the results from three independent mouse models highlighting the podocytes’ independence from mitochondrial energy sources. In contrast, we observed, both *in vitro* and *in vivo*, a strong dependency on cytosolic degradation of glucose to lactate. Neither impaired mitochondrial biogenesis nor defective fission machinery nor mitochondrial transcription resulted in podocyte dysfunction. These experimental findings challenge our view on the mitochondrial contribution to podocyte function and the metabolic status of podocytes in general. Primarily, podocytes do not rely on mitochondrial energy sources under physiological conditions but rather metabolize glucose to lactate instead to meet their energy needs—very similar to Warburg’s hypothesis for cancer cells and many *in vitro* cell culture systems. Podocytes are terminally differentiated quiescent cells. There is accumulating evidence that quiescence is accompanied with strong metabolic changes in order to ensure the maintenance of the cell’s proper function and survival. This metabolic switch from mitochondrial respiration to glycolysis or vice versa is not uniform but rather depends on the cell type and cell environmental context (reviewed in Valcourt et al., 2012). For instance, hematopoietic cells dependence on glycolysis for energy production is related to their localization in a hypoxic niche in the bone marrow (Simsek et al., 2010). Nephron progenitors’ localization in hypoxic niche also appears to be strongly related to

Figure 5. Podocyte-Specific *Pgc-1 α* Knockout Mice Are Viable and Do Not Display a Glomerular Phenotype

(A) Schematic illustrating targeted gene deletion approach of *Pgc-1 α* in podocytes using the Cre-loxP system.

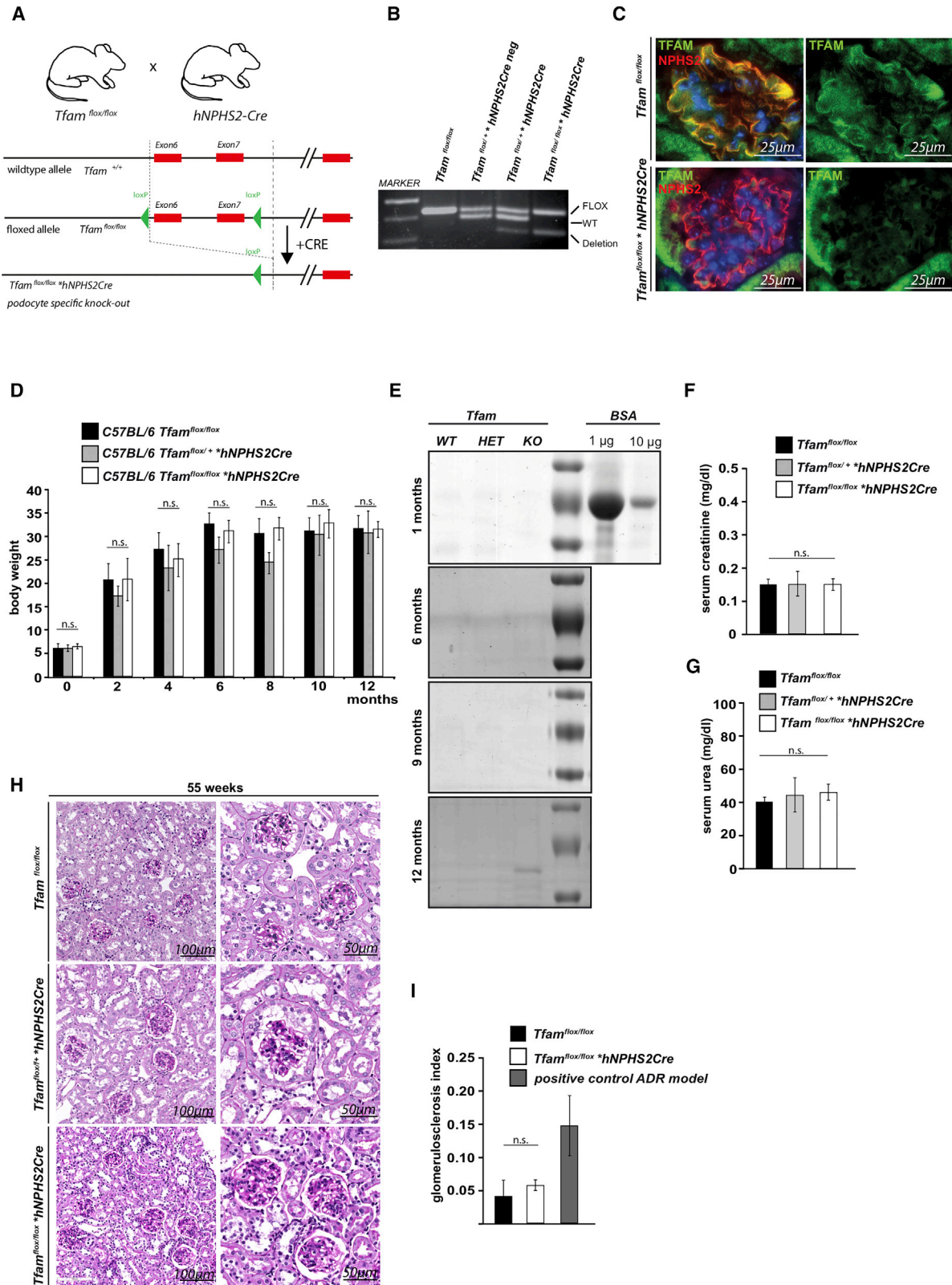
(B) After isolation of podocytes via antibody-based labeling followed by FACS, DNA was prepared and respective genotypes were verified using the following primers: *Pgc-1 α* WT: forward 5'-ACCTGTCTTGCCTATGATTC-3', reverse CCAGTTTCTTCATTGGTGTG; *Pgc-1 α* KO forward 5'-TCCAGTAGGCAGAGATTATGAC-3', reverse 5'-CCAACTGTCTATAATTCCAGTTC-3'.

(C) In a 22-month follow-up period, no differences in body weight were detected between wild-type and *Pgc-1 α* knockout animals (at least 3 animals per genotype and time point were analyzed; mean \pm SD).

(D) Measurement of ACR revealed no differences during the 22-month follow-up period (at least 3 animals per genotype and time point were analyzed; mean \pm SD).

(E) PAS-stained kidney sections from 3-month-old and 22-month-old *Pgc-1 α ^{fllox/fllox}hNPHS2Cre* mice and littermate controls showed normal glomerular structure.

(F) TEM images obtained from 22-month-old *Pgc-1 α ^{fllox/fllox}hNPHS2Cre* and littermate controls show normal foot process formation and no difference in mitochondrial shape (representative pictures).



(legend on next page)

glomerulogenesis through HIF-1a and HIF-2a possible interaction with VEGF (reviewed in Hemker et al., 2016).

We hypothesize that podocytes counteract cellular acidification due to the accumulation of lactate by secretion into the primary urine surrounding the podocytes' cell bodies. The most convincing evidence to support our hypothesis and the independence of podocytes from mitochondrial ATP production comes from clinical observations. Acute kidney injury (AKI) is defined as progressive loss of renal function within hours and often occurs due to a sudden decrease in renal blood flow, leading to kidney ischemia. Patients suffering from AKI usually present with elevated blood urea nitrogen and creatinine levels and a reduction in urine output. Rarely, increased levels of albuminuria are observed, excluding a significant contribution of the glomerular filtration barrier to the course of disease.

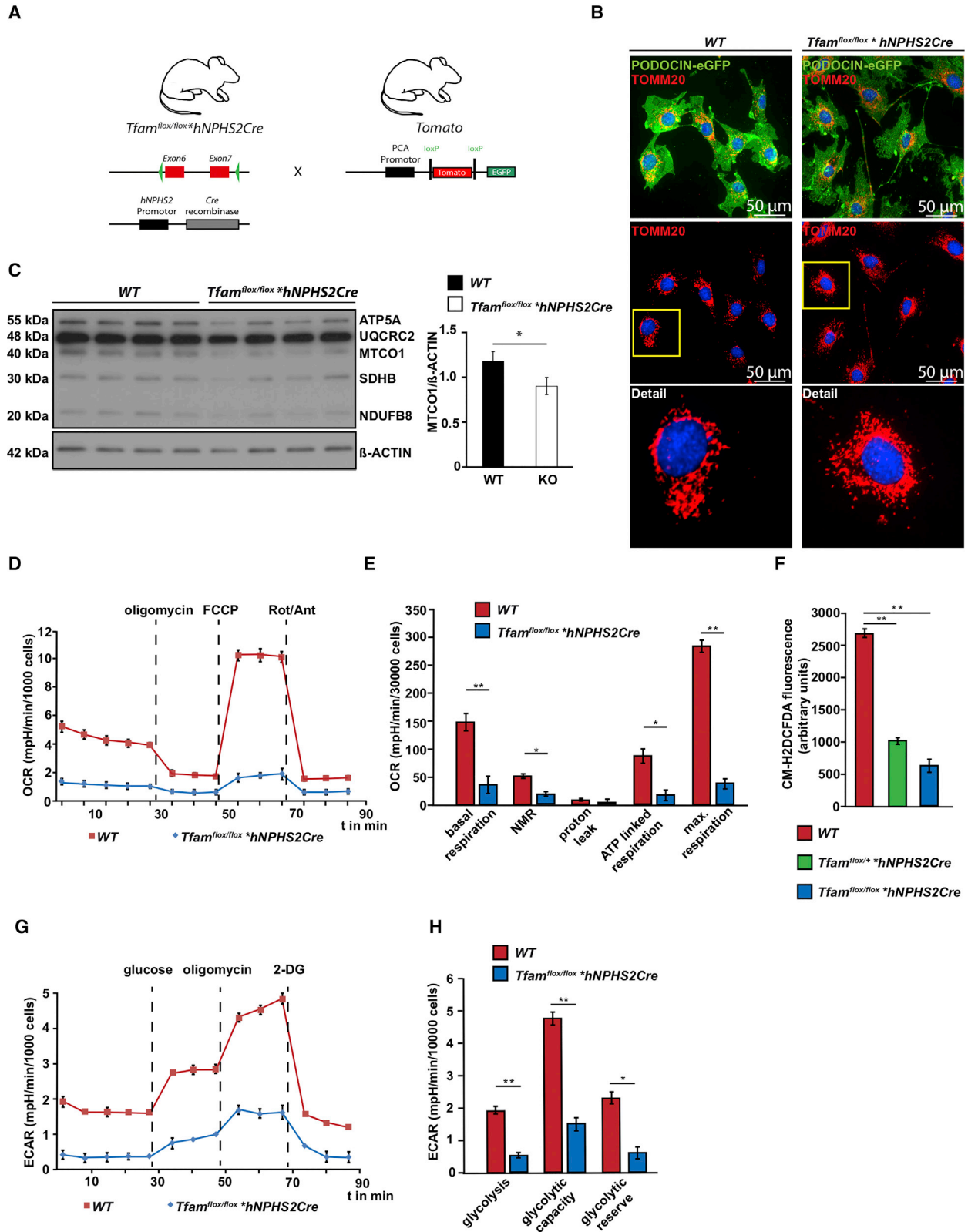
Based on our experimental data, we now speculate that not the loss of mitochondrial OXPHOS is detrimental for podocyte function and, eventually, survival but rather a change in podocyte metabolism. The impact of *Drp1*, *Pgc-1 α* , or *Tfam* depletion on mitochondrial function and podocyte metabolism was only minor, with the strongest changes in overall metabolite content toward increased anaerobic glycolysis being observed in the TFAM-deficient podocytes. Overall, these observations suggest a fully compensated metabolic state due to increased anaerobic glycolysis in these models if mitochondria become genetically targeted.

In the light of recent data, we speculate that mitochondria are critical regulators of metabolic signaling events in podocytes, with mTOR being the ultimate cellular effector kinase (Fantus et al., 2016; Grahammer et al., 2014). Mice with a genetic ablation of prohibitin-2, a scaffold protein in the inner mitochondrial membrane that does not affect the OXPHOS machinery, displayed a severe glomerular disease phenotype and premature death after 4 or 5 weeks, which could be ameliorated by interfering with the insulin-signaling cascade and its downstream mediator mTOR (Ising et al., 2015). Similarly, a transgenic mouse model with genetic activation of mTOR resulted in increased metabolic signaling and the onset of FSGS (Zschiedrich et al., 2017). Notably, the knockout of mTORC1 by induced deletion of both *Raptor* alleles was also found to be detrimental and led to an accelerated progression of FSGS. In contrast, lowering mTORC1 activity by genetic depletion of one *Raptor* allele

ameliorated the progression of glomerulosclerosis in various disease models (Gödel et al., 2011; Zschiedrich et al., 2017). Taken together, these findings lead to the hypothesis that mTOR serves as key regulator of podocyte metabolism without affecting the preferences for the used metabolic pathways. We did not observe a compensatory upregulation of the mitochondrial OXPHOS machinery in the absence of neither *Pgc-1 α* nor *Drp1*. We can only speculate on the observed decrease in glycolysis in *Tfam* knockout (KO) podocytes. This effect could reflect the reduced CO₂ emission by the OXPHOS machinery—also it contributes only very little to the overall ATP content. However, it could also be secondary to the cell isolation protocol, which may result in cellular stress—a condition during which the mitochondrial OXPHOS machinery is required to ascertain cellular function and survival, even though we did not observe an increased rate of cell death in the *Tfam* knockout cells as compared to the control cells. The metabolic framework characterized in this study primarily reflects podocyte metabolism under physiological, non-stressed conditions. It provides an experimental basis to extend our understanding on the mitochondrial contribution to podocyte diseases. The independence of mitochondrial ATP production under physiological conditions not only represents a functional reserve in post-mitotic podocytes but furthermore serves as intracellular source for increased amounts of reactive oxygen species and thereby, ultimately, increased cellular damage and podocyte loss as reported for diabetic nephropathy as a result of hyperglycemia (Ayanga et al., 2016; Chung et al., 2003; Eid et al., 2009; Lee et al., 2003). Along these lines, Qi and colleagues reported in 2017 (Qi et al., 2017) a differential upregulation of enzymes in the glycolytic, sorbitol, methylglyoxal, and mitochondrial pathways to be protective in the setting of diabetic kidney disease. In particular, activation of PKM2 was shown to be protective against diabetic nephropathy (DN) by increasing glucose metabolic flux, inhibiting the production of toxic glucose metabolites and inducing mitochondrial biogenesis to restore mitochondrial function. Hence, a differential and well-orchestrated regulation of multiple signal pathways is required to overcome the deleterious effects of increased mitochondrial ROS, which is distinct from the basal independence of podocytes on the mitochondrial ATP, content. Interfering with the production or scavenging of ROS might represent suitable therapeutic strategies to treat

Figure 6. Podocyte-Specific *Tfam* Knockout Mice Do Not Develop Glomerular Disease

- (A) Schematic illustrating targeted gene deletion approach of *Tfam* in podocytes using the Cre-loxP system.
- (B) After isolation of glomeruli, DNA was prepared and respective genotypes were verified using following primers: *Tfam* forward 5'-CTGCCTCCTAGCCCGG-3'; *Tfam* reverse 1 5'-GTAACAGCAGACAACCTTGTG-3'; *Tfam* reverse 2 5'-CTCTGAAGCACATGGTCAAT-3'.
- (C) Immunofluorescence staining for TFAM in kidney sections obtained from 3-month-old *Tfam^{flox/flox}hNPFS2Cre* mice and respective controls.
- (D) 12-month follow-up period revealed no differences in body weight between wild-type, *Tfam^{flox/+}hNPFS2Cre* mice and *Tfam^{flox/flox}hNPFS2Cre* mice (at least 3 animals per genotype and time point were analyzed; mean \pm SD).
- (E) Urinary protein excretion was absent during a 12-month follow-up period in *Tfam^{flox/flox}*, *Tfam^{flox/+}hNPFS2Cre* mice and *Tfam^{flox/flox}hNPFS2Cre*, respectively, as indicated by representative Coomassie brilliant blue staining.
- (F) Serum creatinine levels in 6-month-old *Tfam^{flox/flox}*, *Tfam^{flox/+}hNPFS2Cre* mice and *Tfam^{flox/flox}hNPFS2Cre* mice, respectively (n = 4 each genotype; mean \pm SD).
- (G) Serum urea levels in 6-month-old *Tfam^{flox/flox}*, *Tfam^{flox/+}hNPFS2Cre* mice and *Tfam^{flox/flox}hNPFS2Cre* mice, respectively (n = 4 each genotype; mean \pm SD).
- (H) PAS-stained kidney sections obtained from 55-week-old *Tfam^{flox/flox}*, *Tfam^{flox/+}hNPFS2Cre* mice and *Tfam^{flox/flox}hNPFS2Cre* mice, respectively.
- (I) Glomerulosclerosis assessment in kidney sections obtained from 55-week-old *Tfam^{flox/flox}* and *Tfam^{flox/flox}hNPFS2Cre* mice, as proposed by el Nahas et al. (1991). Adriamycin-induced nephropathy in WT mice (ICR-CD1 background sacrificed 50 days after induction) served as positive control (n = 3 each group; 100 glomeruli were assessed per mouse; mean \pm SD).



(legend on next page)

patients with DN (Bhatti and Usman, 2015). Activation of the Nrf2/Keap1 pathway by small molecules may serve as one example currently undergoing extensive clinical testing (de Haan, 2011). There is additional, mostly circumstantial data from *in vitro* and *in vivo* models, suggesting a contribution of OXPHOS pathways to the development of podocyte disease. In particular, increased activity of PGC-1 α and, as a result, increased mitochondrial biogenesis has been reported to contribute to the development of collapsing glomerulopathy (Li et al., 2017), and it appeared to be protective in a model of aldosterone-induced podocyte injury (Zhao et al., 2016). Hyperglycemia itself has been reported to activate podocyte metabolism by inducing DRP1-mediated mitochondrial fission through ROCK1 (Wang et al., 2012). As it relates to TFAM and the role of mtDNA stability and mtDNA transcription, very little is known about its importance for kidney cells although global deletion of *Tfam* was embryonically lethal (Larsson et al., 1998). Kidneys from heterozygous *Tfam*^{+/-} mice present with mtDNA depletion that is not followed by OXPHOS deficiency (Larsson et al., 1998). Moreover, TFAM overexpression in mice leads to mtDNA copy number increase in all tissues—including kidney—without affecting mtDNA expression and OXPHOS function (Ekstrand et al., 2004). Conditional disruption of *Tfam* expression in heart and skeletal muscle cells resulted in a severe phenotype and death of the animals after 2–4 weeks of age (Wang et al., 1999), although loss of TFAM in epidermal progenitor/stem cells (EPSCs) had no effect on epidermal development and skin barrier function (Baris et al., 2011), very similar to the lack of any disease phenotype as reported for podocytes in this study. Differential regulation of the different complexes of the OXPHOS machinery in the absence of TFAM, including the nuclear-encoded genes of complex II as observed in this study and also by Vernochet et al. (2012) in brown adipose tissue, may contribute to the tissue-specific consequences of a targeted *Tfam* deletion, ranging from the absence of any phenotype to embryonic lethality.

In conclusion, this study provides insights into podocyte metabolism as podocytes primarily rely on anaerobic glycolysis and only to a minor extent on β -oxidation of lipids. Overall, mitochondrial oxidative phosphorylation has only very limited impact on the overall podocyte ATP synthesis. As such, anaerobic glycolysis and the fermentation of glucose to lactate is the predominant metabolic pathway of podocytes and therefore represents a key target for therapeutic interventions in glomerular disease with enhanced metabolism, such as diabetic nephropathy.

STAR★METHODS

Detailed methods are provided in the online version of this paper and include the following:

- KEY RESOURCES TABLE
- CONTACT FOR REAGENT AND RESOURCE SHARING
- EXPERIMENTAL MODEL AND SUBJECT DETAILS
 - Animals
 - Primary Cell Culture
- METHOD DETAILS
 - Urine and serum analysis
 - Histology and electron microscopy
 - *Ex vivo* podocyte isolation and DNA isolation and PCR
 - Staining of podocytes and ROS detection
 - Immunofluorescence staining
 - Cell and glomerular lysis and western blot procedure
 - qPCR for mitochondrial and nuclear DNA targets
 - Seahorse XFp mitochondrial analysis and ATP measurement
 - GC/MS based untargeted metabolomics screen
- QUANTIFICATION AND STATISTICAL ANALYSIS
 - Statistical analysis

SUPPLEMENTAL INFORMATION

Supplemental Information can be found online at <https://doi.org/10.1016/j.celrep.2019.04.012>.

ACKNOWLEDGMENTS

This study was supported by the Deutsche Forschungsgemeinschaft (DFG) (German Research Foundation): Clinical research unit (KFO 329, BR 2955/8-1 to P.T.B., SCHE 1562/7-1 to B.S., and BE 2212/23-1 and 2212/24-1 to T. Benzing), collaborative research centers (SFB/CRC) 1140 (project number 246781735 to T.B.H.), CRC 1192 (to T.B.H.) and CRC 992 (to T.B.H.), Heisenberg Program (to T.B.H.), and HU 1016/8-2 (to T.B.H.); the European Research Council (ERC grant to T.B.H.) and by the H2020-IMI2 consortium BEAT-DKD and this Joint undertaking receives support from the European Union's Horizon 2020 research and innovation program and EFPIA with JDRF (115974; to T.B.H.); by the Bundesministerium für Bildung und Forschung, STOP Fokale Segmentale Glomerulosklerose (BMBF-STOP-FSGS) 01GM1518C (to T.B.H.); by the Excellence Initiative of the German Federal and State Governments (BLOSS to T.B.H.); the Freiburg Institute for Advanced Studies (to T.B.H.); the National Natural Science Foundation of China (81470912 to W.L.); the Berta Ottenstein Programm (to C.S.); the Else Kröner Fresenius Stiftung, Nierenfunktionsstörungen als Komplikation von Systemerkrankungen (NAKSYS) (to T. Bork, C.S., and T.B.H.); and the Alexander von Humboldt Foundation

Figure 7. Metabolic Profiling of *Tfam*-Deficient Podocytes Revealed Decreased Respiratory Activity

- (A) Schematic illustrating breeding strategy to generate primary podocytes lacking *Tfam*.
 (B) Immunofluorescence image obtained from primary podocytes deficient for *Tfam* and controls shows a comparable distribution and intensity for the mitochondrial marker TOMM20 (red).
 (C) Western blot analysis for key components of the respiratory chain revealed lower levels of MTCO1 in *Tfam*-deficient podocytes (n = 4; *p ≤ 0.05; mean ± SD).
 (D) OCR from *Tfam*-deficient podocytes and controls at baseline and after subsequent injection of oligomycin, FCCP, and rotenone, and rotenone, antimycin A (mean ± SD). Final concentration: oligomycin: 1 μM; FCCP: 0.5 μM; rotenone: 0.5 μM; antimycin: 0.5 μM.
 (E) Statistics of key parameters of respiratory function in *Tfam*-deficient podocytes and controls (*p ≤ 0.05; **p ≤ 0.01; mean ± SD).
 (F) Quantitative CM-H2DCFDA fluorescence obtained from primary podocytes with complete or heterozygous disruption of *Tfam* and controls, indicating oxidative stress (**p ≤ 0.01; ***p ≤ 0.001; mean ± SD).
 (G) Extracellular acidification rate of *Tfam*-deficient podocytes and respective controls followed after glucose administration and subsequent injection of oligomycin and 2-DG (mean ± SD). Final concentration: glucose: 10 mM; oligomycin: 1 μM; 2-DG: 50 mM.
 (H) Statistics of key parameters of glycolytic activity obtained from *Tfam*-deficient podocytes and respective controls (*p ≤ 0.05; **p ≤ 0.01; mean ± SD).

and National Health and Medical Research Council of Australia Research Fellowships (to V.G.P.).

AUTHOR CONTRIBUTIONS

Conceptualization, P.T.B. and T.B.H.; Methodology, C.H., T. Bork, and C.I.; Investigation, A.A., A.M., C.I., A.K., B.K., C.Ö., C.S., H.H.H., T. Bork, M.S., O.K., S.L., S.K., S. Salou, S. Schnyder, V.G.P., and W.L.; Writing – Original Draft, P.T.B., C.H., C.S., and T.B.H.; Review & Editing, B.S. and T. Benzing; Funding Acquisition, P.T.B., C.H., C.S., and T.B.H.; Study Initiation & Supervision, T.B.H.

DECLARATION OF INTERESTS

The authors declare no competing interests.

Received: April 9, 2018

Revised: March 13, 2019

Accepted: April 2, 2019

Published: April 30, 2019

REFERENCES

- Abe, Y., Sakairi, T., Kajiyama, H., Shrivastav, S., Beeson, C., and Kopp, J.B. (2010). Bioenergetic characterization of mouse podocytes. *Am. J. Physiol. Cell Physiol.* 299, C464–C476.
- Ayanga, B.A., Badal, S.S., Wang, Y., Galvan, D.L., Chang, B.H., Schumacker, P.T., and Danesh, F.R. (2016). Dynamin-related protein 1 deficiency improves mitochondrial fitness and protects against progression of diabetic nephropathy. *J. Am. Soc. Nephrol.* 27, 2733–2747.
- Baris, O.R., Klose, A., Klopper, J.E., Weiland, D., Neuhaus, J.F., Schauen, M., Wille, A., Müller, A., Merkwirth, C., Langer, T., et al. (2011). The mitochondrial electron transport chain is dispensable for proliferation and differentiation of epidermal progenitor cells. *Stem Cells* 29, 1459–1468.
- Bartlett, C.S., Jeansson, M., and Quaggin, S.E. (2016). Vascular growth factors and glomerular disease. *Annu. Rev. Physiol.* 78, 437–461.
- Bhatti, A.B., and Usman, M. (2015). Drug targets for oxidative podocyte injury in diabetic nephropathy. *Cureus* 7, e393.
- Bratic, A., and Larsson, N.G. (2013). The role of mitochondria in aging. *J. Clin. Invest.* 123, 951–957.
- Brinkkoetter, P.T., Ising, C., and Benzing, T. (2013). The role of the podocyte in albumin filtration. *Nat. Rev. Nephrol.* 9, 328–336.
- Che, R., Yuan, Y., Huang, S., and Zhang, A. (2014). Mitochondrial dysfunction in the pathophysiology of renal diseases. *Am. J. Physiol. Renal Physiol.* 306, F367–F378.
- Chung, S.S., Ho, E.C., Lam, K.S., and Chung, S.K. (2003). Contribution of polyol pathway to diabetes-induced oxidative stress. *J. Am. Soc. Nephrol.* 14, S233–S236.
- de Haan, J.B. (2011). Nrf2 activators as attractive therapeutics for diabetic nephropathy. *Diabetes* 60, 2683–2684.
- de Jong, P.E., and Curhan, G.C. (2006). Screening, monitoring, and treatment of albuminuria: Public health perspectives. *J. Am. Soc. Nephrol.* 17, 2120–2126.
- Detmer, S.A., and Chan, D.C. (2007). Functions and dysfunctions of mitochondrial dynamics. *Nat. Rev. Mol. Cell Biol.* 8, 870–879.
- Doleris, L.M., Hill, G.S., Chedin, P., Nochy, D., Bellanne-Chantelot, C., Hanslik, T., Bedrossian, J., Caillat-Zucman, S., Cahen-Varsaux, J., and Bariety, J. (2000). Focal segmental glomerulosclerosis associated with mitochondrial cytopathy. *Kidney Int.* 58, 1851–1858.
- Eid, A.A., Gorin, Y., Fagg, B.M., Maalouf, R., Barnes, J.L., Block, K., and Abboud, H.E. (2009). Mechanisms of podocyte injury in diabetes: role of cytochrome P450 and NADPH oxidases. *Diabetes* 58, 1201–1211.
- Ekstrand, M.I., Falkenberg, M., Rantanen, A., Park, C.B., Gaspari, M., Hulthén, K., Rustin, P., Gustafsson, C.M., and Larsson, N.G. (2004). Mitochondrial transcription factor A regulates mtDNA copy number in mammals. *Hum. Mol. Genet.* 13, 935–944.
- el Nahas, A.M., Bassett, A.H., Cope, G.H., and Le Carpentier, J.E. (1991). Role of growth hormone in the development of experimental renal scarring. *Kidney Int.* 40, 29–34.
- Fantus, D., Rogers, N.M., Grahammer, F., Huber, T.B., and Thomson, A.W. (2016). Roles of mTOR complexes in the kidney: implications for renal disease and transplantation. *Nat. Rev. Nephrol.* 12, 587–609.
- Gödel, M., Hartleben, B., Herbach, N., Liu, S., Zschiedrich, S., Lu, S., Debreczeni-Mór, A., Lindenmeyer, M.T., Rastaldi, M.P., Hartleben, G., et al. (2011). Role of mTOR in podocyte function and diabetic nephropathy in humans and mice. *J. Clin. Invest.* 121, 2197–2209.
- Grahammer, F., Wanner, N., and Huber, T.B. (2014). mTOR controls kidney epithelia in health and disease. *Nephrol. Dial. Transplant.* 29 (Suppl 1), i9–i18.
- Hemker, S.L., Sims-Lucas, S., and Ho, J. (2016). Role of hypoxia during nephrogenesis. *Pediatr. Nephrol.* 31, 1571–1577.
- Hotta, O., Inoue, C.N., Miyabayashi, S., Furuta, T., Takeuchi, A., and Taguma, Y. (2001). Clinical and pathologic features of focal segmental glomerulosclerosis with mitochondrial tRNA^{Leu}(UUR) gene mutation. *Kidney Int.* 59, 1236–1243.
- Imasawa, T., and Rossignol, R. (2013). Podocyte energy metabolism and glomerular diseases. *Int. J. Biochem. Cell Biol.* 45, 2109–2118.
- Imasawa, T., Obre, E., Bellance, N., Lavie, J., Imasawa, T., Rigother, C., Delmas, Y., Combe, C., Lacombe, D., Benard, G., et al. (2017). High glucose repatterns human podocyte energy metabolism during differentiation and diabetic nephropathy. *FASEB J.* 31, 294–307.
- Ising, C., Koehler, S., Brähler, S., Merkwirth, C., Höhne, M., Baris, O.R., Hagmann, H., Kann, M., Fabretti, F., Dafinger, C., et al. (2015). Inhibition of insulin/IGF-1 receptor signaling protects from mitochondria-mediated kidney failure. *EMBO Mol. Med.* 7, 275–287.
- Kers, J., Leemans, J.C., and Linkermann, A. (2016). An overview of pathways of regulated necrosis in acute kidney injury. *Semin. Nephrol.* 36, 139–152.
- Kurogouchi, F., Oguchi, T., Mawatari, E., Yamaura, S., Hora, K., Takei, M., Sekijima, Y., Ikeda, S., and Kiyosawa, K. (1998). A case of mitochondrial cytopathy with a typical point mutation for MELAS, presenting with severe focal-segmental glomerulosclerosis as main clinical manifestation. *Am. J. Nephrol.* 18, 551–556.
- Larsson, N.G., Wang, J., Wilhelmsson, H., Oldfors, A., Rustin, P., Lewandoski, M., Barsh, G.S., and Clayton, D.A. (1998). Mitochondrial transcription factor A is necessary for mtDNA maintenance and embryogenesis in mice. *Nat. Genet.* 18, 231–236.
- Lee, H.B., Yu, M.R., Yang, Y., Jiang, Z., and Ha, H. (2003). Reactive oxygen species-regulated signaling pathways in diabetic nephropathy. *J. Am. Soc. Nephrol.* 14 (8, Suppl 3), S241–S245.
- Li, S.Y., Park, J., Qiu, C., Han, S.H., Palmer, M.B., Arany, Z., and Susztak, K. (2017). Increasing the level of peroxisome proliferator-activated receptor γ co-activator-1 α in podocytes results in collapsing glomerulopathy. *JCI Insight* 2, 92930.
- Lin, J., Wu, P.H., Tarr, P.T., Lindenberg, K.S., St-Pierre, J., Zhang, C.Y., Mootha, V.K., Jäger, S., Vianna, C.R., Reznick, R.M., et al. (2004). Defects in adaptive energy metabolism with CNS-linked hyperactivity in PGC-1 α null mice. *Cell* 119, 121–135.
- Miner, J.H. (2012). The glomerular basement membrane. *Exp. Cell Res.* 318, 973–978.
- Moeller, M.J., Sanden, S.K., Soofi, A., Wiggins, R.C., and Holzman, L.B. (2003). Podocyte-specific expression of cre recombinase in transgenic mice. *Genesis* 35, 39–42.
- Müller-Deile, J., and Schiffer, M. (2014). The podocyte power-plant disaster and its contribution to glomerulopathy. *Front. Endocrinol. (Lausanne)* 5, 209.
- Nunnari, J., and Suomalainen, A. (2012). Mitochondria: in sickness and in health. *Cell* 148, 1145–1159.

- O'Toole, J.F. (2014). Renal manifestations of genetic mitochondrial disease. *Int. J. Nephrol. Renovasc. Dis.* **7**, 57–67.
- Osman, C., Voelker, D.R., and Langer, T. (2011). Making heads or tails of phospholipids in mitochondria. *J. Cell Biol.* **192**, 7–16.
- Ozawa, S., Ueda, S., Imamura, H., Mori, K., Asanuma, K., Yanagita, M., and Nakagawa, T. (2015). Glycolysis, but not Mitochondria, responsible for intracellular ATP distribution in cortical area of podocytes. *Sci. Rep.* **5**, 18575.
- Peti-Peterdi, J., and Sipos, A. (2010). A high-powered view of the filtration barrier. *J. Am. Soc. Nephrol.* **21**, 1835–1841.
- Pinto-Sietsma, S.J., Janssen, W.M., Hillege, H.L., Navis, G., De Zeeuw, D., and De Jong, P.E. (2000). Urinary albumin excretion is associated with renal functional abnormalities in a nondiabetic population. *J. Am. Soc. Nephrol.* **11**, 1882–1888.
- Qi, W., Keenan, H.A., Li, Q., Ishikado, A., Kannt, A., Sadowski, T., Yorek, M.A., Wu, I.H., Lockhart, S., Coppey, L.J., et al. (2017). Pyruvate kinase M2 activation may protect against the progression of diabetic glomerular pathology and mitochondrial dysfunction. *Nat. Med.* **23**, 753–762.
- Raimundo, N. (2014). Mitochondrial pathology: stress signals from the energy factory. *Trends Mol. Med.* **20**, 282–292.
- Raimundo, N., Song, L., Shutt, T.E., McKay, S.E., Cotney, J., Guan, M.X., Gilliland, T.C., Hohuan, D., Santos-Sacchi, J., and Shadel, G.S. (2012). Mitochondrial stress engages E2F1 apoptotic signaling to cause deafness. *Cell* **148**, 716–726.
- Saleem, M.A., O'Hare, M.J., Reiser, J., Coward, R.J., Inward, C.D., Faren, T., Xing, C.Y., Ni, L., Mathieson, P.W., and Mundel, P. (2002). A conditionally immortalized human podocyte cell line demonstrating nephrin and podocin expression. *J. Am. Soc. Nephrol.* **13**, 630–638.
- Schell, C., Baumhagl, L., Salou, S., Conzelmann, A.C., Meyer, C., Helmstädter, M., Wrede, C., Grahammer, F., Eimer, S., Kerjaschki, D., et al. (2013). N-wasp is required for stabilization of podocyte foot processes. *J. Am. Soc. Nephrol.* **24**, 713–721.
- Schmidt, O., Pfanner, N., and Meisinger, C. (2010). Mitochondrial protein import: from proteomics to functional mechanisms. *Nat. Rev. Mol. Cell Biol.* **11**, 655–667.
- Simsek, T., Kocabas, F., Zheng, J., Deberardinis, R.J., Mahmoud, A.I., Olson, E.N., Schneider, J.W., Zhang, C.C., and Sadek, H.A. (2010). The distinct metabolic profile of hematopoietic stem cells reflects their location in a hypoxic niche. *Cell Stem Cell* **7**, 380–390.
- Singer, M.A. (2001). Of mice and men and elephants: metabolic rate sets glomerular filtration rate. *Am. J. Kidney Dis.* **37**, 164–178.
- Valcourt, J.R., Lemons, J.M., Haley, E.M., Kojima, M., Demuren, O.O., and Collier, H.A. (2012). Staying alive: metabolic adaptations to quiescence. *Cell Cycle* **11**, 1680–1696.
- Vernochet, C., Mourier, A., Bezy, O., Macotela, Y., Boucher, J., Rardin, M.J., An, D., Lee, K.Y., Ilkayeva, O.R., Zingaretti, C.M., et al. (2012). Adipose-specific deletion of TFAM increases mitochondrial oxidation and protects mice against obesity and insulin resistance. *Cell Metab.* **16**, 765–776.
- von Kleist-Retzow, J.C., Hornig-Do, H.T., Schauen, M., Eckertz, S., Dinh, T.A., Stassen, F., Lottmann, N., Bust, M., Galunski, B., Wielckens, K., et al. (2007). Impaired mitochondrial Ca²⁺ homeostasis in respiratory chain-deficient cells but efficient compensation of energetic disadvantage by enhanced anaerobic glycolysis due to low ATP steady state levels. *Exp. Cell Res.* **313**, 3076–3089.
- Wakabayashi, J., Zhang, Z., Wakabayashi, N., Tamura, Y., Fukaya, M., Kensler, T.W., Iijima, M., and Sesaki, H. (2009). The dynamin-related GTPase Drp1 is required for embryonic and brain development in mice. *J. Cell Biol.* **186**, 805–816.
- Wang, J., Wilhelmsson, H., Graff, C., Li, H., Oldfors, A., Rustin, P., Brünig, J.C., Kahn, C.R., Clayton, D.A., Barsh, G.S., et al. (1999). Dilated cardiomyopathy and atrioventricular conduction blocks induced by heart-specific inactivation of mitochondrial DNA gene expression. *Nat. Genet.* **21**, 133–137.
- Wang, W., Wang, Y., Long, J., Wang, J., Haudek, S.B., Overbeek, P., Chang, B.H., Schumacker, P.T., and Danesh, F.R. (2012). Mitochondrial fission triggered by hyperglycemia is mediated by ROCK1 activation in podocytes and endothelial cells. *Cell Metab.* **15**, 186–200.
- Willmann, L., Schlimpert, M., Halbach, S., Erbes, T., Stickeler, E., and Kamberer, B. (2015). Metabolic profiling of breast cancer: differences in central metabolism between subtypes of breast cancer cell lines. *J. Chromatogr. B Analyt. Technol. Biomed. Life Sci.* **1000**, 95–104.
- Xia, J., and Wishart, D.S. (2016). Using MetaboAnalyst 3.0 for comprehensive metabolomics data analysis. *Curr. Protoc. Bioinformatics* **55**, 14.10.1–14.10.91.
- Yamagata, K., Muro, K., Usui, J., Hagiwara, M., Kai, H., Arakawa, Y., Shimizu, Y., Tomida, C., Hirayama, K., Kobayashi, M., and Koyama, A. (2002). Mitochondrial DNA mutations in focal segmental glomerulosclerosis lesions. *J. Am. Soc. Nephrol.* **13**, 1816–1823.
- Zhao, M., Yuan, Y., Bai, M., Ding, G., Jia, Z., Huang, S., and Zhang, A. (2016). PGC-1 α overexpression protects against aldosterone-induced podocyte depletion: role of mitochondria. *Oncotarget* **7**, 12150–12162.
- Zschiedrich, S., Bork, T., Liang, W., Wanner, N., Eulenbruch, K., Munder, S., Hartleben, B., Kretz, O., Gerber, S., Simons, M., et al. (2017). Targeting mTOR signaling can prevent the progression of FSGS. *J. Am. Soc. Nephrol.* **28**, 2144–2157.

STAR★METHODS

KEY RESOURCES TABLE

REAGENT or RESOURCE	SOURCE	IDENTIFIER
Antibodies		
anti-podocin	Sigma	P0372
anti-TOMM20	Santa Cruz	sc-11415
anti-TFAM	Santa Cruz	sc-23588
anti-DRP1	BD Transduction	611112
anti-NEPHRIN	Progen	GP-N2
anti-SYNAPOPODIN	Synapotic Systems	163 004
anti-PKM2	Cell Signaling	D78A4
anti-SOD2	Acris Antibodies	APO3023PU-S
anti-alpha TUBULIN	Sigma	T6199
anti-PGC-1a	Merck Milipore	4C1.3
OXPHOS Rodent WB Antibody Cocktail	Abcam	Ab110413
anti-ATP	Abcam	AB113849
Bacterial and Virus Strains		
Chemicals, Peptides, and Recombinant Proteins		
CM-H2DCFDA	Invitrogen	C6827
oligomycin	Sigma	75351
FCCP	Sigma	C2920
antimycin A	Sigma	A8674
rotenone	Abcam	Ab14315
etomoxir	Sigma	E1905
BPTES	Sigma	SML0601
UK5099	Sigma	PZ0160
2-DG	Sigma	D6134
oxamate	Sigma	O2751
Critical Commercial Assays		
Seahorse XFp Mito Fluor Flex Test	Agilent Technologies	N/A
Mito Stress Test	Agilent Technologies	N/A
Seahorse XF Glycolysis Stress Test Kit	Agilent Technologies	N/A
Experimental Models: Cell Lines		
Immortalized human podocytes	Saleem et al., 2002	N/A
Experimental Models: Organisms/Strains		
B6.129S4(FVB)-Ppargc1atm1Brsp/J	Lin et al., 2004	N/A
B6.Drp1flox/flox/J	Wakabayashi et al., 2009	N/A
B6.Tfamflox/flox/N	Larsson et al., 1998	N/A
B6.hNPHS2Cre	Moeller et al., 2003	N/A
Gt(ROSA)26Sortm4(ACTB-tdTomato,-EGFP)Luo/J	Jackson Laboratory	N/A
Oligonucleotides		
Tfam forward 5'-CTGCCCTCCTAGCCCGG-3'	Larsson et al., 1998	N/A
Tfam reverse 1 5'-GTAACAGCAGACAACCTGTG-3'	Larsson et al., 1998	N/A
Tfam reverse 2 5'-CTCTGAAGCACATGGTCAAT-3'	Larsson et al., 1998	N/A
Pgc-1 α WT: frwd 5'-ACCTGTCTTTGCCTATGATTC	Lin et al., 2004	N/A
Pgc-1 α WT: reverse 5'-CCAGTTTCTTCATTGGTGTG -3'	Lin et al., 2004	N/A
Pgc-1 α KO forward: 5'-TCCAGTA GGCAGAGATTTATGAC-3'	Lin et al., 2004	N/A

(Continued on next page)

Continued

REAGENT or RESOURCE	SOURCE	IDENTIFIER
Pgc-1 α KO reverse: 5'-CCAAGTGTCTATAATTCCAGTTC-3'	Lin et al., 2004	N/A
Drp1: D1 5'-CACTGAGAGCTCTATATGTAGGC-3'	Wakabayashi et al., 2009	N/A
D3 5'-ACCAAAGTAAGGAAT AGCTGTTG-3'	Wakabayashi et al., 2009	N/A
D5 5'-GAGTACCTAAAGTGGACAAGAGGTCC-3'	Wakabayashi et al., 2009	N/A
cox1	Thermo Fisher Scientific	Mm04225243_g1
Atp6	Thermo Fisher Scientific	Mm03649417_g1
18S	Thermo Fisher Scientific	Hs99999901_s1
siRNA Drp1, Pgc1alpha and Tfam	On Target Smart Pool, Dharmacon	N/A
Software and Algorithms		
Imaris software v7.6	Bitplane	N/A
LabImage ID software	Kapelan Bio-Imaging	N/A
Seahorse XFp software version 2.2.0	Seahorse Bioscience	N/A
GraphPad Prism Version 6	GraphPad Software	N/A
MetaboAnalyst	Xia and Wishart, 2016	N/A

CONTACT FOR REAGENT AND RESOURCE SHARING

Further information and requests for resources and reagents should be directed to and will be fulfilled by the Lead Contact, Tobias B. Huber (t.huber@uke.de).

EXPERIMENTAL MODEL AND SUBJECT DETAILS**Animals**

Mice: B6.129S4(FVB)-Ppargc1a^{tm1Brsp/J} were a generous gift from B. Spiegelman ([Lin et al., 2004](#)). *Drp1*^{flox/flox} mice ([Wakabayashi et al., 2009](#)) on C57BL/6J background were a generous gift from H. Sesaki (Johns Hopkins University School of Medicine, Baltimore). *Tfam*^{flox/flox} mice ([Larsson et al., 1998](#)) on C57BL/6N background were a generous gift from N.G. Larsson (Max Planck Institute for Biology of Aging, Cologne/Germany). All mice were backcrossed to pure C57BL/6J or 6N background, respectively. To obtain a podocyte-specific knockout of *Drp1*, *Tfam* and *Pgc-1 α* , respectively, mice harboring the respective floxed allele were further crossed to *hNPHS2Cre* mice provided by L. Holzman (Renal, Electrolyte and Hypertension Division, University of Pennsylvania School of Medicine, Philadelphia, PA, USA) to generate a podocyte specific knockout. Only male mice were phenotypically analyzed (cohort size: *Drp1*: n = 10; *Pgc-1 α* : n = 6, *Tfam*: n = 8; control cohorts (WT) include 10, 6 and 8 mice, respectively). Male *hNPHS2Cre* negative littermates served as controls. All animal experiments were conducted according to the guidelines of the Committee on Research Animal Care and the German and Swiss law for the welfare of animals. All experiments were approved by local authorities (Regierungspraesidium Freiburg (G11/38, G14/45), Kantonales Veterinäramt of the Kanton Basel and the LANUV NRW (State Agency for Nature, Environment and Consumer Protection North Rhine-Westphalia), respectively. Mice had free access to chow and water and a 12-hour day/night cycle. Breeding and genotyping was done according to standard procedures. To isolate primary podocytes *Tfam*^{flox/flox};*hNPHS2Cre*⁺ were crossed to *Tomato/eGFP* reporter mice. Gt(ROSA)26Sortm4(ACTB-tdTomato,-EGFP)Luo/J mice were purchased from Jackson Laboratory (Bar Harbor, ME). *Tfam*^{flox/flox}; *Tomato/eGFP*⁺*hNPHS2Cre*⁺ and *WT*; *Tomato/eGFP*⁺*hNPHS2Cre*⁺ were chosen for primary cell isolation.

Primary Cell Culture

Isolation of primary podocytes was performed as recently described ([Schell et al., 2013](#)). In brief glomeruli from 2 week old *Tfam*^{flox/flox}; *Tomato/eGFP*; *hNPHS2Cre*⁺ and *WT*; *Tomato/eGFP*; *hNPHS2Cre*⁺ mice, respectively, were isolated by sieving. After culture of 5 days FACS procedure was performed to isolate the GFP-positive population of primary podocytes. For all *ex vivo* experiments podocytes were kept in 5.5mM D-glucose reflecting normoglycemic conditions.

METHOD DETAILS**Urine and serum analysis**

Urinary albumin was analyzed with Coomassie gel stains and measured using a fluorimetric albumin test kit (Progen, PR2005). Urinary creatinine was measured using enzymatic colorimetric creatinine kit (Labor+Technik, LT-CR0053) as described in the manufacturer's instructions.

Histology and electron microscopy

Kidneys were fixed in 4% paraformaldehyde and embedded in paraffin and further processed for PAS and HE staining. For quantitative assessment of glomerular lesions as previously described by El Nahas (el Nahas et al., 1991) 2 μ m PAS stained kidney slides of at least 3 animals were analyzed for focal (1 point) or total sclerosis (2 points). The sum was divided by the number of counted glomeruli. This was done in a blinded fashion and repeated by a second renal pathology experienced scientist.

For transmission electron microscopy, tissue blocks were washed after post fixation in 0.1M PB, and sections (thickness: 50 μ m) of the kidney were cut by using vibratome. After incubation in 1% OsO₄, the sections were stained with uranyl acetate, dehydrated and flat embedded in epoxy resin (Durcupan ACM, Fluka, Sigma-Aldrich, Gillingham, UK). 40 nm ultrathin sections were cut and analyzed using an 80kV Zeiss Leo transmission electron microscope.

Ex vivo podocyte isolation and DNA isolation and PCR

To confirm the podocyte-specific knock out of *Tfam*, *Pgc-1 α* and *Drp1*, respectively, podocytes were *ex vivo* isolated after Dynabead perfusion and several digestion steps. Finally, podocytes were captured by anti-podocin antibody (P0372, Sigma) coupled to Alexa Fluor 488 (Z25302, Thermo Scientific) (*Pgc-1 α*) or isolated due to their GFP-signal (*Tfam^{flox/flox};Tomato/eGFP;hNPHS2Cre⁺* and *Drp1^{flox/flox};Tomato/eGFP;hNPHS2Cre⁺* mice). DNA was isolated using DNeasy kit (QIAGEN, 69504) following manufacturer's instructions. PRC was performed using following primers: *Tfam* forward 5'-CTGCCCTCCTAGCCCGG-3', *Tfam* reverse 1 5'-GTAA CAGCAGACAACCTTGTG-3', *Tfam* reverse 2 5'-CTCTGAAGCACATGGTCAAT-3'. *Pgc-1 α* alpha primer: *Pgc-1 α* WT: frwd 5'-ACCT GTCTTTGCCTATGATTC, reverse 5'- CCAGTTTCTTCATTGGTGTG -3'; *Pgc-1 α* KO forward: 5'-TCCAGTA

GGCAGAGATTTATGAC-3', reverse: 5'-CCAAGTGTCTATAATTCCAGTTC-3'.

Drp1: D1 (5'-CACTGAGAGCTCTATATGTAGGC-3'), D3 (5'-ACCAAAGTAAGGAAT AGCTGTTG-3') and D5 (5'-GAGTACCTAAAGTGACAAGAGGTCC-3').

Staining of podocytes and ROS detection

Primary podocytes obtained from *Tfam^{flox/flox};Tomato/eGFP;hNPHS-Cre⁺* and *WT; Tomato/eGFP;hNPHS2Cre⁺* mice were seeded on collagen coated coverslips. 24h later cells were fixed with paraformaldehyde (4% in phosphate buffered saline (PBS)) and stained with rabbit anti TOMM20 (Santa Cruz, sc-11415).

For ROS detection primary podocytes were seeded in a 96 well plate with clear flat bottom and black sides the day before the experiment (25 000 cells/well). After washing podocytes were incubated in 5 μ M working solution of CM-H₂DCFDA (Invitrogen, C6827) at 37°C in the dark. CM-H₂DCFDA was replaced by PBS and excitation/emission was measured (485/535nm) in a plate reader (Tecan Infinite).

Immunofluorescence staining

Tfam^{flox/flox};hNPHS2Cre and *Drp1^{flox/flox};hNPHS2Cre* and respective controls were perfused with phosphate buffered saline (PBS) via cardiac perfusion. For TFAM staining mice kidneys were fixed in 4% formaldehyde, embedded in paraffin and cut in 4 μ m sections. Samples were deparaffinized in xylene and rehydrated in ethanol gradient (100% - 95% - 70%). The slides were washed with TBST (Tris-buffered-saline with 0.025% Tween 20) and boiled in Tris-EDTA pH 9.0 for 10 min to obtain antigen retrieval. After washing with milliQ water and TBST samples were blocked with 5% BSA and 5% normal donkey serum in TBST for 1 hour at room temperature. Incubation with primary antibodies overnight at 4°C was followed by secondary antibodies for 60 min at room temperature. Following antibodies were used: anti mtTFA (A-17) (Santa Cruz, sc-23588), anti PODOCIN (Sigma, P0372). Imaging was performed with a Leica DMI 6000 B inverted microscope - HCX PL APO 63x/1.40 oil immersion objective. All images were further processed with the CorelDRAW(R) Graphics Suite X6.

For DRP1 staining, kidneys were snap-frozen in cryogenic Tissue-Tek O.C.T. compound (Electron Microscopy Sciences) and 4 μ m cryosections were generated with a Leica Kryostat (Leica, Wetzlar, Germany). Sections were fixed with PFA 4%, followed by treatment with NH₄CL (50 mM) and blocking with 5% BSA in PBS. Subsequently the sections were incubated with following primary antibodies for 60 minutes: anti-DRP1 (BD Transduction) and anti-NEPHRIN (guinea pig, 1:300, Progen) After several rinses, appropriate fluorophore-conjugated Alexa secondary antibodies (Invitrogen) in a final dilution of 1:500 were applied for 30 minutes. Images were taken using a Zeiss fluorescence microscope.

For localization studies of glycolysis (assessed for PKM2 distribution) and mitochondrial distribution (assessed for SOD) indirect immunofluorescence was performed following the protocol described above. Podocytes were identified using synaptopodin (Synaptic Systems; 163 004), glycolytic enzyme abundance was assessed via PKM2 (Cell Signaling Technology D78A4) and mitochondrial distribution was visualized via SOD2 expression (Acris Antibodies; APO3023PU-S). Image acquisition was performed using a scanning confocal microscope (LSM800, Zeiss) with airy scan function, which allowed image post processing. 3D reconstructions, distributions and volumetric calculations (i.e., maximal distance to podocyte nuclei) were performed based on 6 stacks per group by using Imaris software v7.6 (Bitplane).

Cell and glomerular lysis and western blot procedure

Glomeruli were isolated by Dynabead perfusion. Cells were harvested by trypsinization and lysis was performed using RIPA buffer. Protein concentration was determined by BCA assay (Pierce Biotechnology, 23225). Equal amounts of protein were separated on

SDS-PAGE. Afterward, gels were transferred to a polyvinylidene difluoride membrane (iBlot Gel Transfer Stacks, Life Technologies, IB401001) by dry blotting technique (iBlot® 2 Dry Blotting System, Life technologies). Membranes were blocked in 5% PBS-BSA. Following antibodies were used for western blot: anti β -ACTIN (Sigma, A9357), anti-alpha TUBULIN (Sigma, T6199), anti DRP-1 (Cell Signaling Technology, D6C7), anti TFAM (Abcam, ab131607), anti PGC-1 α (Merck Millipore, 4C1.3), total OXPHOS Rodent WB Antibody Cocktail (Abcam, ab110413). Densitometry was performed using LabImage ID software (Kapelan Bio-Imaging).

qPCR for mitochondrial and nuclear DNA targets

DNA was extracted out of *ex vivo* isolated glomeruli (Dynabead perfusion for high purity, 4 mice per genotype at the age of 24 weeks) using the QIAGEN DNeasy Blood & Tissue kit according to the manufacturer's instructions and total concentrations were measured with the Thermo Fisher NanoDrop spectrophotometer. DNA was diluted to 2,5ng/ μ l and the individual dilution factors were noted down. mtDNA copy numbers were assessed by conducting qPCR, in which 18S was used for measurement of genomic DNA and served as loading control and Rnr2 and cox1 were used for measuring mitochondrial genes (Thermo Fisher Scientific, cox1: Mm04225243_g1; Atp6: Mm03649417_g1; 18S: Hs99999901_s1). Measurements were compared to five standard dilutions, ranging from undiluted to the highest dilution factor used when diluting the DNA isolated out of podocytes. Four technical replicates were measured per sample.

Seahorse XFp mitochondrial analysis and ATP measurement

Optimization of cell density for primary podocytes as well as optimization of the working concentration titers for each individual inhibitor was conducted prior to the Seahorse XFp experiments according to the manufacturer's instructions (Agilent Technologies). Cells were seeded at a density of 20 000 cells/well. The Seahorse XFp Mito Fuel Flex Test, Mito Stress Test and assessment of glycolytic activity was performed following the manufacturer's instruction. Specifically, podocytes on XFp microplates were rinsed. XF assay buffer was added. Afterward the plate was equilibrated for 1 h at 37°C in a non-CO₂ incubator. All medium and solutions of mitochondrial complex inhibitors were adjusted to pH 7.4 on the day of assay. Following four baseline measurements of OCR and ECAR, inhibitors of the respiratory chain were sequentially injected into each well. Three OCR and ECAR readings were taken after addition of each inhibitor and before automated injection of the subsequent inhibitor. Mitochondrial complex inhibitors, in order of injection, included oligomycin (1 μ M) to inhibit complex V, FCCP (0.5 μ M) to uncouple the proton gradient, antimycin A (1.0 μ M, inhibitor of complex III), and rotenone (1.0 μ M, complex I inhibitor). For Mito Fuel assessment etomoxir, BPTES, UK5099 were used with final concentration of 100 μ M (etomoxir) and 30 μ M (BPTES, UK5099). OCR and ECAR were automatically calculated by Seahorse XFp software version 2.2.0 (Seahorse Bioscience, Billerica, MA, USA). After each experiment podocytes were fixed with paraformaldehyde and nuclei were stained with DAPI. Olympus ScanR Screening Station for high-throughput microscopy detection (Olympus, Tokyo, Japan) was used for assessment of cell number to normalize XFp analysis data.

Knock-down experiments for *Drp1*, *Pgc-1 α* and *Tfam*, respectively, were performed in immortalized human podocytes (kindly provided by Moin Saleem (Bristol, UK)) (Saleem et al., 2002). Podocytes were seeded in RPMI 1640 supplemented with 10% FCS, Insulin/Transferrin/Selenite, Penicillin/Streptomycin (all from Roche Diagnostics, Mannheim, Germany), Pyruvate, 100x Minimal Essential Medium and HEPES Buffer (all Life technologies, Darmstadt, Germany). When cells had grown to 60% confluence differentiation was induced at 37.0°C for 10–14 days. Cultured human podocytes were fully differentiated before any experiment.

Knock-down experiments for *Drp1*, *Pgc-1 α* and *Tfam*, respectively, were performed by using predesigned pooled siRNA (four targeting one gene, On target SMART pool, Dharmacon). Transfection was performed by using electroporation (Amaxa nucleofector technology, Lonza) according to manufacturer's instructions. Efficiency of the knockdown was confirmed 48 hours after transfection using western blot. The Seahorse XFp Mito Fuel Flex Test, Mito Stress Test and assessment of glycolytic activity was performed 48h after transfection.

For ATP measurement primary podocytes were treated with 2-DG (50 mM), oxamate (45 mM), etomoxir (100 μ M) and oligomycin (1 μ M) and ATP measurement was performed using luminescent ATP detection (Abcam 113849) following the manufacturer's instructions.

GC/MS based untargeted metabolomics screen

Glomeruli were *ex vivo* harvested using Dynabead perfusion. Tubular compartment was isolated by microdissection. To assess the impact of *Drp1*, *Pgc-1 α* and *Tfam* deletion, respectively, on metabolite profiles, kidney cortex obtained from 24-week-old mice from each genotype and respective controls were analyzed (n = 4 each). All tissue preparation was performed on ice in less than 30 s. Metabolites were extracted in 90% methanol and 10% water at –20°C containing 1 μ g/ml ribitol and 1 μ g/ml phenylglucose as internal standards. Tissue lysis was performed by using a Precellys 24 homogenizer with screw cap vials prefilled with 300 mg glass beads (diameter 600 μ m) as follows: two times three cycles of 30 s homogenization and 30 s break at –20°C. Further sample processing and metabolic profiling was conducted as described by Willmann et al. (2015). In summary, after centrifugation, metabolite containing supernatant was dried overnight and the pellet was derivatized by methoxyamination and silylation. Untargeted GC/MS profiling was performed with a 30 m HP5-MS column coupled to an electron impact mass spectrometer. Features were deconvoluted, aligned and annotated according to mass spectral similarity and retention index of three different libraries. The principal component analysis (PCA) and heatmap were generated by MetaboAnalyst (Xia and Wishart, 2016).

QUANTIFICATION AND STATISTICAL ANALYSIS

Statistical analysis

Results of all experiments are presented as mean \pm SD. To test for statistical significance of observed effects two-tailed t test was used calculated with GraphPad Prism (Version 6, GraphPad Software, La Jolla, California, USA). p value \leq 0.05 represented statistically significant differences.

Cell Reports, Volume 27

Supplemental Information

Anaerobic Glycolysis Maintains the Glomerular Filtration Barrier Independent of Mitochondrial Metabolism and Dynamics

Paul T. Brinkkoetter, Tillmann Bork, Sarah Salou, Wei Liang, Athanasia Mizi, Cem Özel, Sybille Koehler, H. Henning Hagmann, Christina Ising, Alexander Kuczkowski, Svenia Schnyder, Ahmed Abed, Bernhard Schermer, Thomas Benzing, Oliver Kretz, Victor G. Puelles, Simon Lagies, Manuel Schlimpert, Bernd Kammerer, Christoph Handschin, Christoph Schell, and Tobias B. Huber

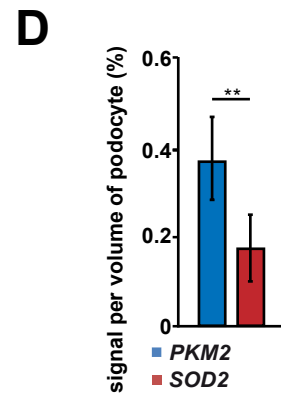
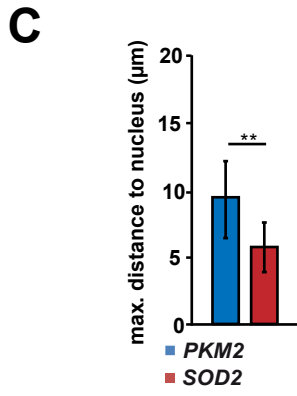
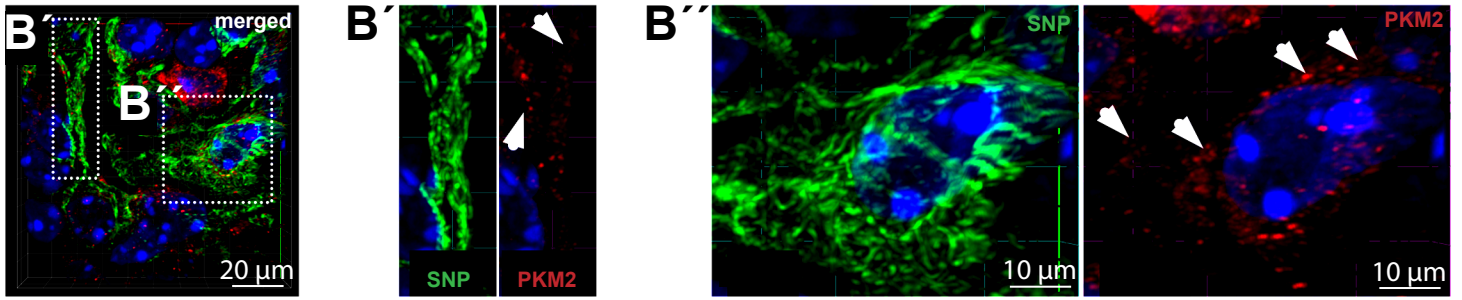
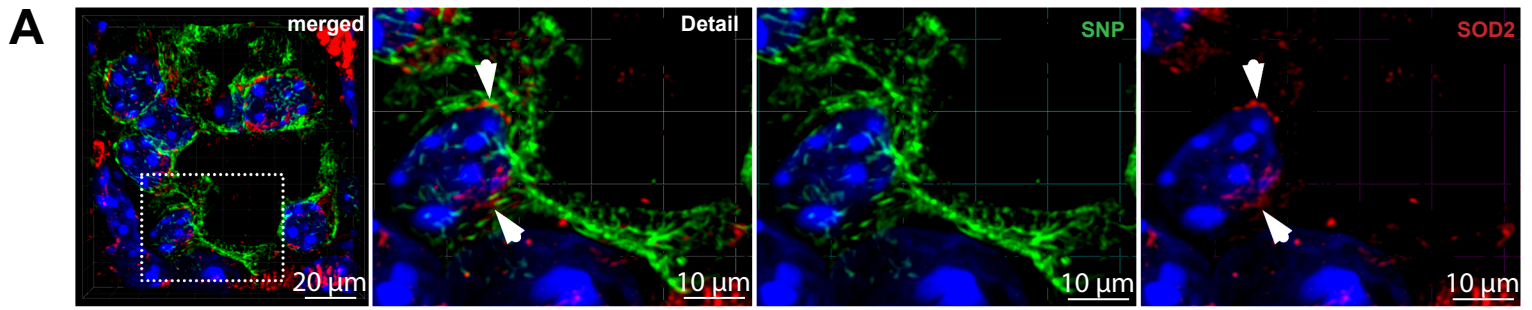


Figure S1: Mitochondria were primarily found within the cytoplasm and primary processes of podocytes, Related to Figure 1

(A) Immunofluorescence image obtained from mouse glomeruli (8 weeks old) for synaptopodin (green, podocyte marker) and SOD2 (red, mitochondrial enzyme). Arrowheads point to mitochondrial signal.

(B) Immunofluorescence image obtained from mouse glomeruli (8 weeks old) for synaptopodin (green, podocyte marker) and PKM2 (red, glycolytic enzyme). Arrowheads in the high magnification point to PKM2 signal, primarily found in foot processes.

(C) Quantification of the maximal distance of SOD2 and PKM2 signal to the nucleus (obtained from 20 glomeruli).

(D) Quantification of the volume of SOD2 and PKM2 signal compared to podocyte volume (obtained from 20 glomeruli).

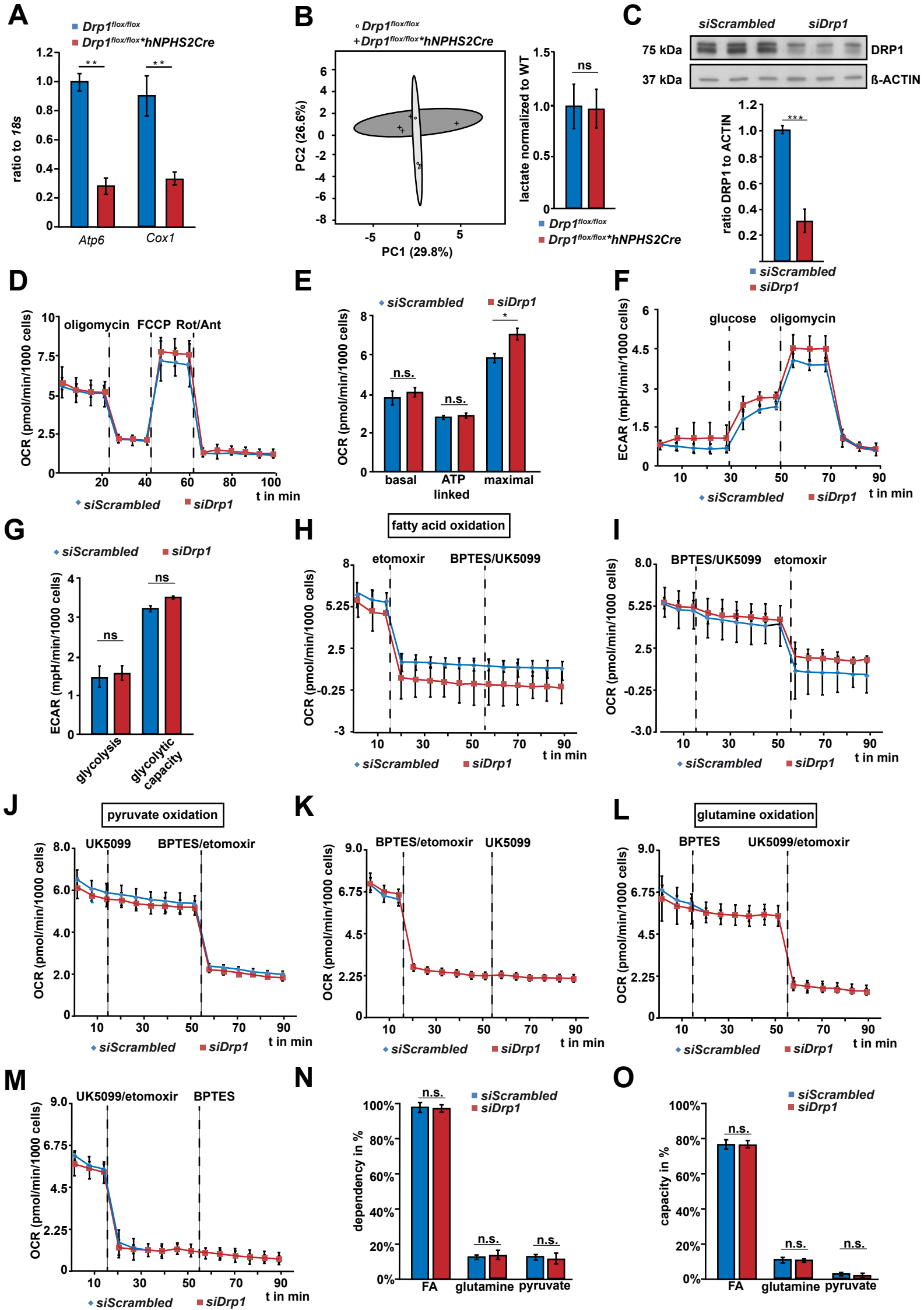


Figure S2: Impact of *Drp1* deletion on the expression of mitochondria encoded genes and function, Related to Figure 4

(A) qPCR for the abundance of mitochondrial DNA (Atp6, Cox I) normalized to genomic DNA (18s) (p-value ** ≤ 0.01).

(B) Principal component analysis of metabolite abundance from kidney cortex obtained from 24-week-old mice of respective genotype assessed by unbiased GC-MS based metabolomic analysis (n=4 each group). Lactate levels normalized to WT.

(C) Western blot and densitometry for the abundance of DRP1 in human podocytes after siRNA-based knock-down compared to scrambled siRNA controls (p-value *** ≤ 0.001).

(D) Mitochondrial function of human podocytes after knock-down of *Drp1* and respective controls. Oxygen consumption rate (OCR) was measured at basal level and after the sequential addition of oligomycin (1 mM), FCCP (0.5 mM), and rotenone (Rot; 1.0 mM) + antimycin A (Ant; 1.0 mM; n=3, technical replicates).

(E) Combined results underline the minor role of *Drp1* for mitochondrial respiratory function as shown for basal respiration, ATP-linked oxygen consumption rate and maximal respiratory capacity (p-value * ≤ 0.05).

(F) Extracellular acidification rate (ECAR) of human podocytes with knock-down of *Drp1* and respective controls at baseline and after injection of glucose followed by oligomycin.

(G) Combined results underline the minor impact of *Drp1* for anaerobic utilization of glucose as shown for glycolysis and maximal glycolytic capacity.

(H) Dependency of fatty acid oxidation of human podocytes with knock-down for *Drp1* and respective controls obtained after etomoxir and BPTES/UK5099 injection. Final concentrations: etomoxir: 100 μ M, BPTES: 30 μ M, UK5099: 30 μ M.

(I) Capacity of fatty acid oxidation of human podocytes with knock-down for *Drp1* and respective controls obtained after BPTES/UK5099 injection followed by etomoxir, Final concentrations: etomoxir: 100 μ M, BPTES: 30 μ M, UK5099: 30 μ M.

(J) Dependency of pyruvate oxidation of human podocytes with knock-down for *Drp1* and respective controls obtained after UK5099 and BPTES/etomoxir injection. Final concentrations: UK5099: 30 μ M, etomoxir: 100 μ M, BPTES: 30 μ M.

(K) Capacity of pyruvate oxidation of human podocytes with knock-down for *Drp1* and respective controls obtained after BPTES/etomoxir and UK5099 injection. Final concentrations: etomoxir: 100 μ M, BPTES: 30 μ M, UK5099: 30 μ M.

(L) Dependency of glutamine oxidation of human podocytes with knock-down for *Drp1* and respective controls obtained after BPTES and UK5099/etomoxir injection. Final concentrations: BPTES: 30 μ M, UK5099: 30 μ M, etomoxir: 100 μ M.

(M) Capacity of glutamine oxidation of human podocytes with knock-down for *Drp1* and respective controls obtained after UK5099/etomoxir and BPTES injection. Final concentrations: UK5099: 30 μ M, etomoxir: 100 μ M, BPTES: 30 μ M.

(N) Statistics for substrate dependency of human podocytes with knock-down for *Drp1* and respective controls.

(O) Statistics for substrate capacity of human podocytes with knock-down for *Drp1* and respective controls.

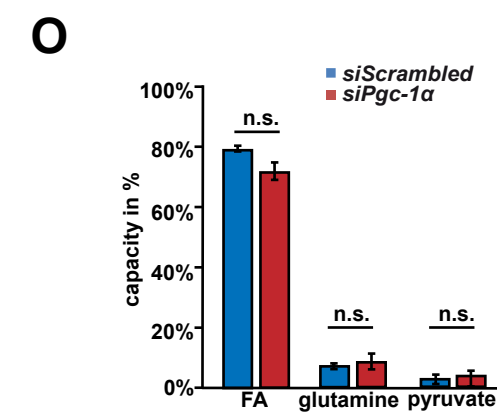
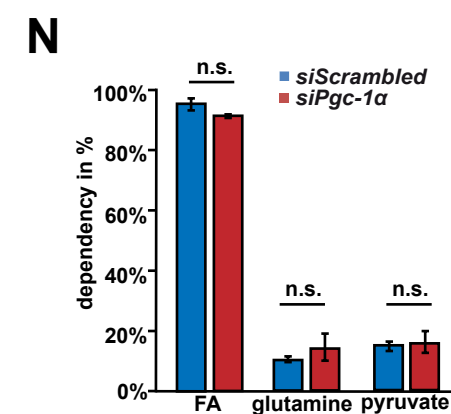
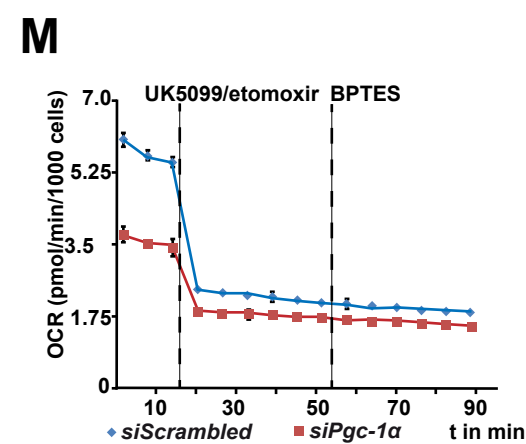
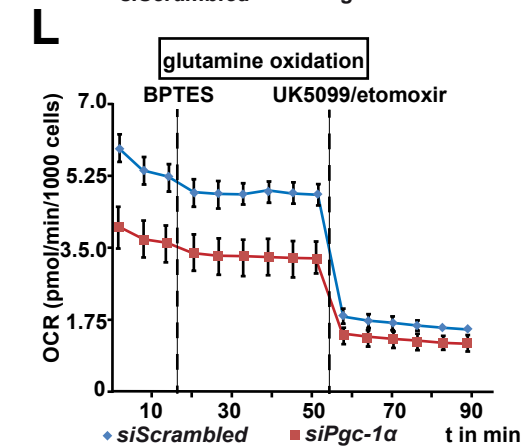
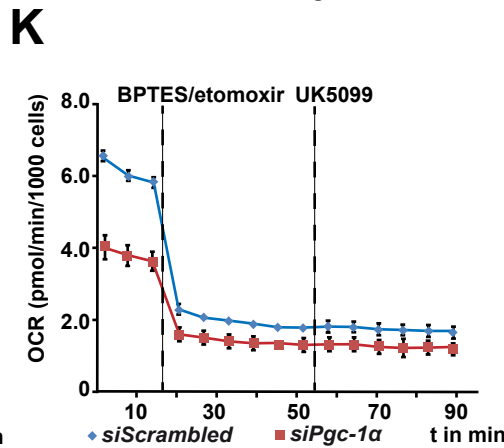
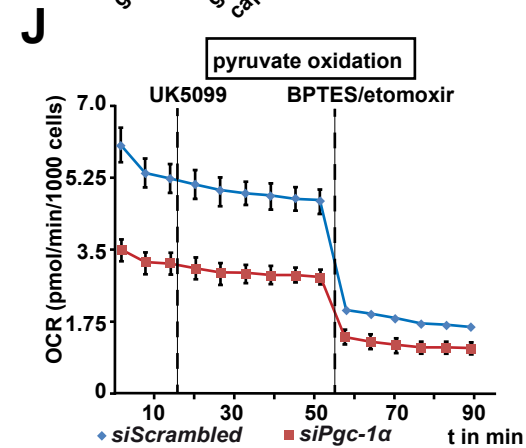
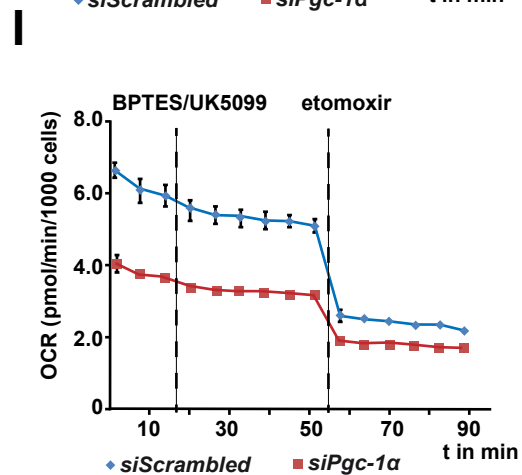
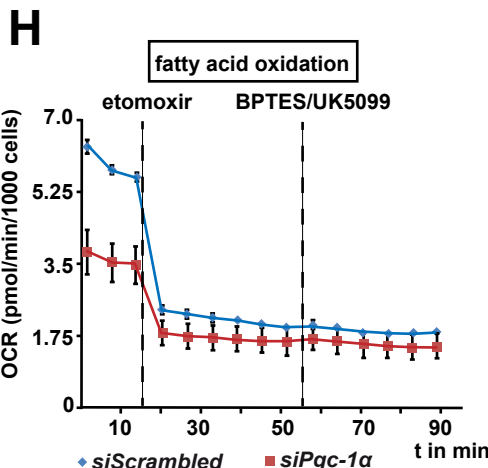
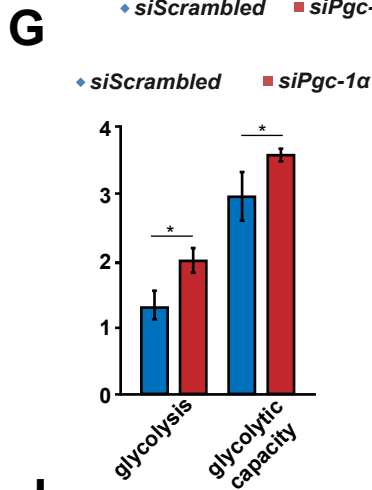
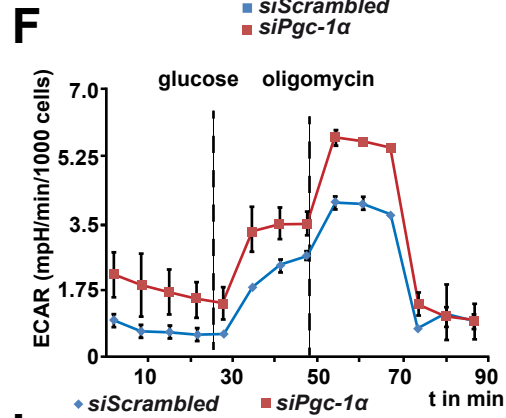
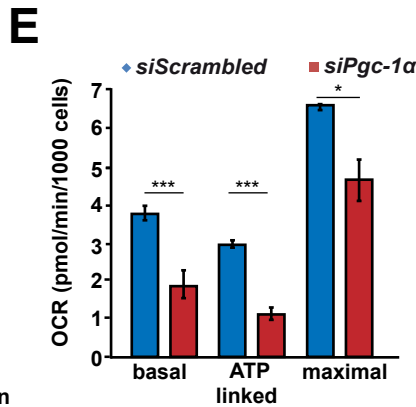
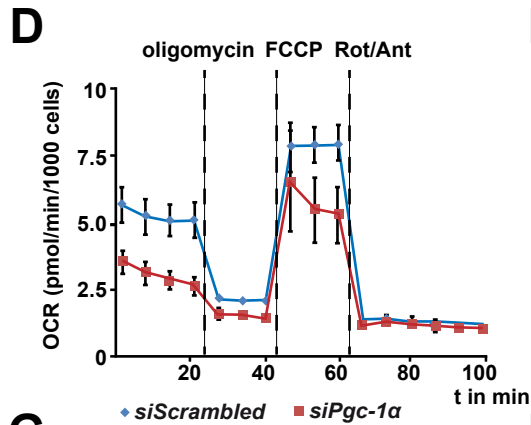
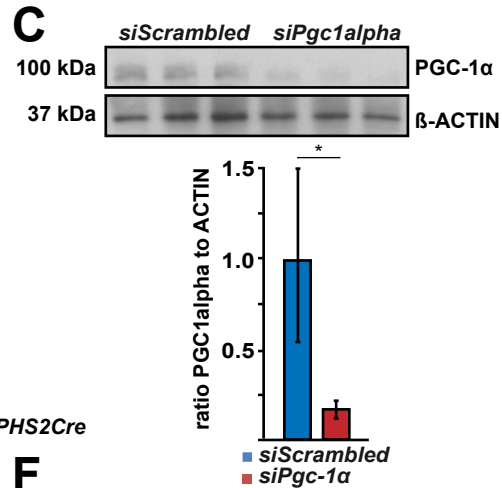
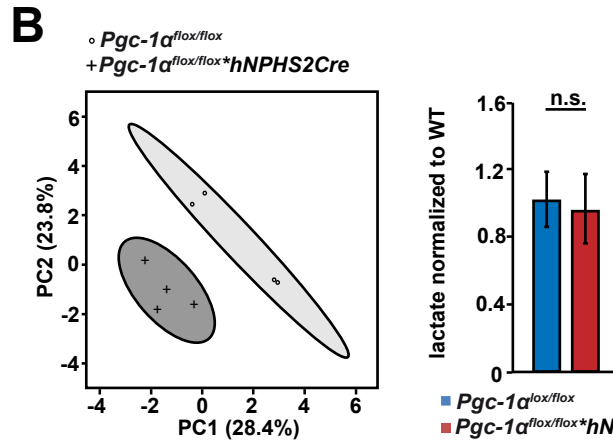
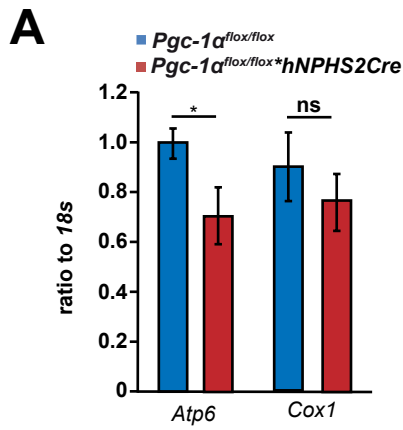


Figure S3: Impact of *Pgc-1 α* deletion on the expression of mitochondria encoded genes and function, Related to Figure 5

(A) qPCR for the abundance of mitochondrial DNA (Atp6, Cox I) normalized to genomic DNA (18s) (p-value * ≤ 0.05).

(B) Principal component analysis of metabolite abundance from kidney cortex obtained from 24-week-old mice of respective genotype assessed by unbiased GC-MS based metabolomic analysis (n=4 each group). Lactate levels normalized to WT.

(C) Western blot and densitometry for the abundance of PGC-1 α in human podocytes after siRNA-based knock-down compared to scrambled siRNA controls (p-value * ≤ 0.05).

(D) Mitochondrial function of human podocytes after knock-down of *Pgc-1 α* and respective controls. Oxygen consumption rate (OCR) was measured at basal level and after the sequential addition of oligomycin (1 mM), FCCP (0.5 mM), and rotenone (Rot; 1.0 mM) + antimycin A (Ant; 1.0 mM; n=3, technical replicates).

(E) Combined results underline the major role of *Pgc-1 α* for mitochondrial respiratory function as shown for basal respiration, ATP-linked oxygen consumption rate and maximal respiratory capacity (p-value * ≤ 0.05 and *** ≤ 0.001).

(F) Extracellular acidification rate (ECAR) of human podocytes with knock-down of *Pgc-1 α* and respective controls at baseline and after injection of glucose followed by oligomycin.

(G) Combined results underline the major impact of *Pgc-1 α* for anaerobic utilization of glucose as shown for glycolysis and maximal glycolytic capacity (p-value * ≤ 0.05).

(H) Dependency of fatty acid oxidation of human podocytes with knock-down for *Pgc-1 α* and respective controls obtained after etomoxir and BPTES/UK5099 injection. Final concentrations: etomoxir: 100 μ M, BPTES: 30 μ M, UK5099: 30 μ M.

(I) Capacity of fatty acid oxidation of human podocytes with knock-down for *Pgc-1 α* and respective controls obtained after BPTES/UK5099 injection followed by etomoxir, Final concentrations: etomoxir: 100 μ M, BPTES: 30 μ M, UK5099: 30 μ M.

(J) Dependency of pyruvate oxidation of human podocytes with knock-down for *Pgc-1 α* and respective controls obtained after UK5099 and BPTES/etomoxir injection. Final concentrations: UK5099: 30 μ M, etomoxir: 100 μ M, BPTES: 30 μ M.

(K) Capacity of pyruvate oxidation of human podocytes with knock-down for *Pgc-1 α* and respective controls obtained after BPTES/etomoxir and UK5099 injection. Final concentrations: etomoxir: 100 μ M, BPTES: 30 μ M, UK5099: 30 μ M.

(L) Dependency of glutamine oxidation of human podocytes with knock-down for *Pgc-1 α* and respective controls obtained after BPTES and UK5099/etomoxir injection. Final concentrations: BPTES: 30 μ M, UK5099: 30 μ M, etomoxir: 100 μ M.

(M) Capacity of glutamine oxidation of human podocytes with knock-down for *Pgc-1 α* and respective controls obtained after UK5099/etomoxir and BPTES injection. Final concentrations: UK5099: 30 μ M, etomoxir: 100 μ M, BPTES: 30 μ M.

(N) Statistics for substrate dependency of human podocytes with knock-down for *Pgc-1 α* and respective controls.

(O) Statistics for substrate capacity of human podocytes with knock-down for *Pgc-1 α* and respective controls.

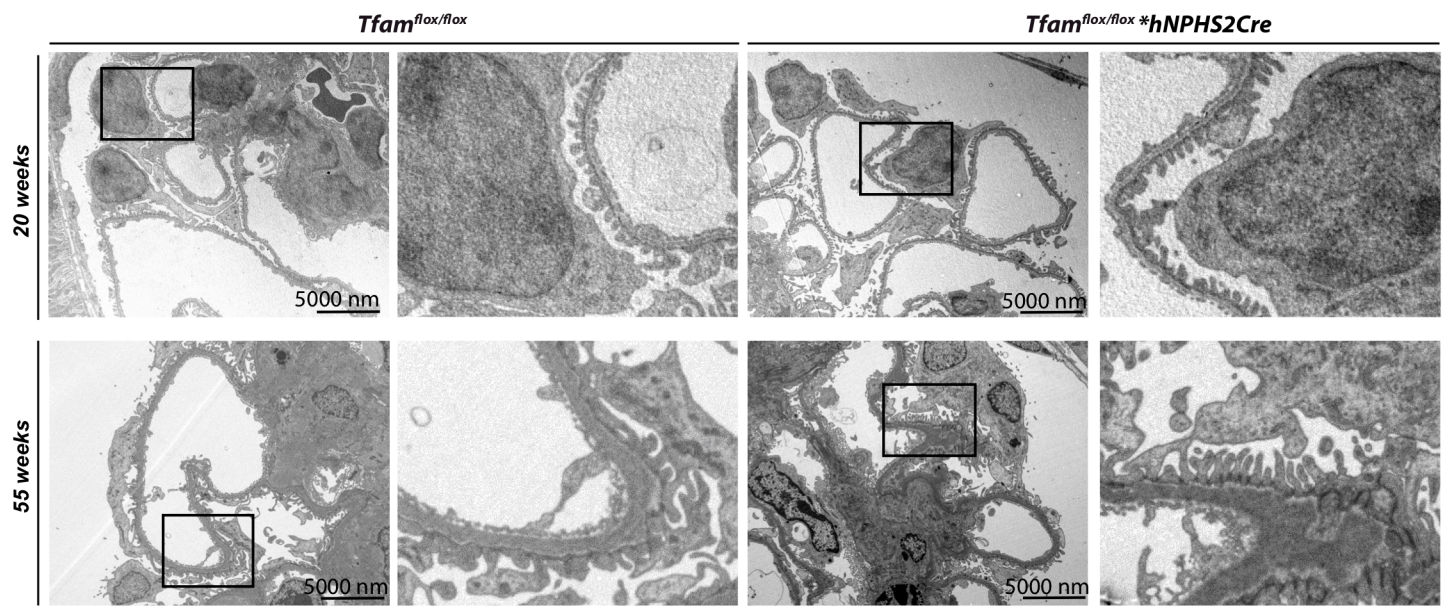
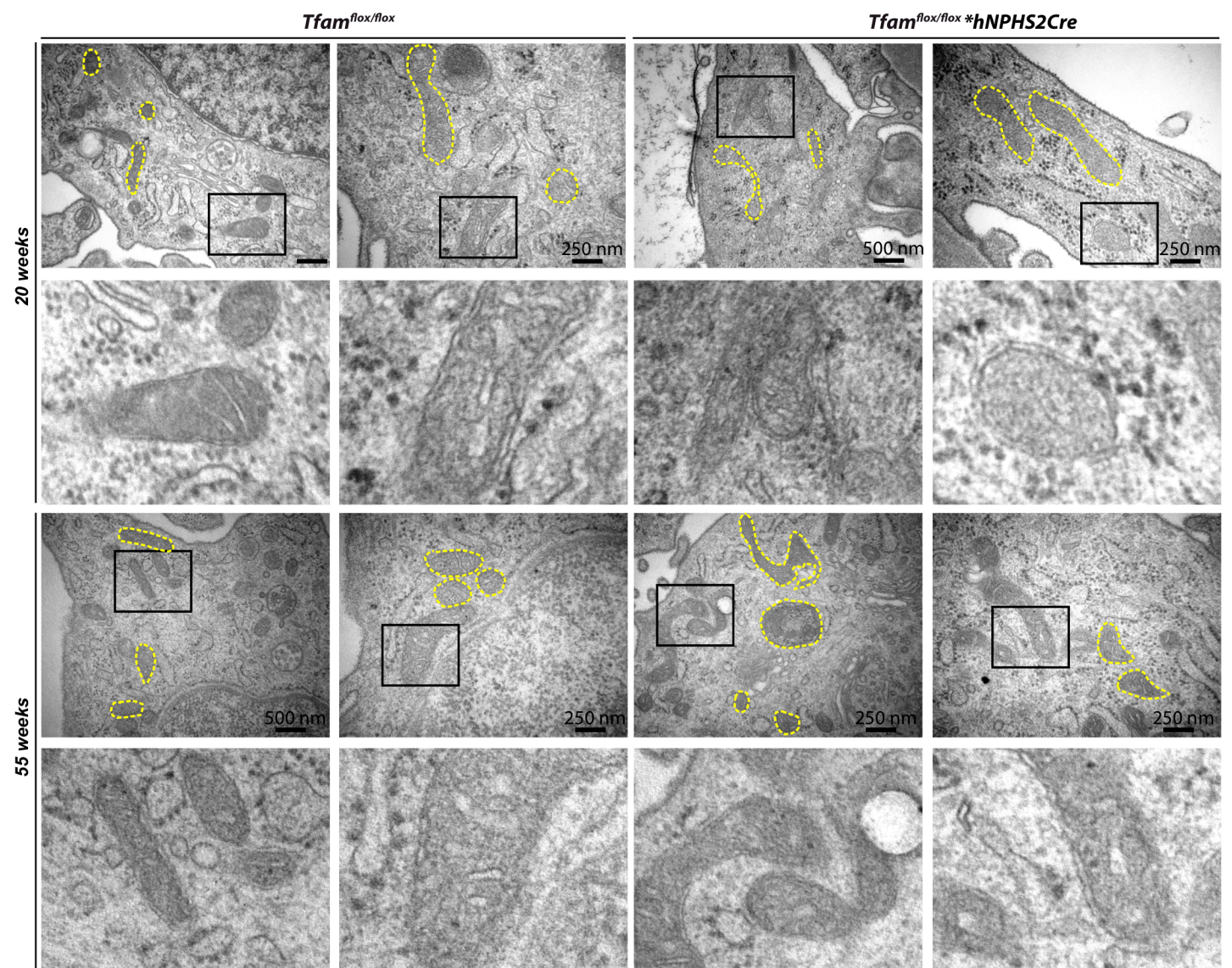
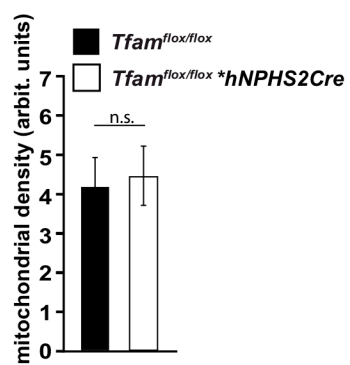
A**B****C**

Figure S4: Podocyte-specific *Tfam* knockout mice do not develop glomerular disease, Related to Figure 6

Podocyte-specific *Tfam* knockout mice do not develop glomerular disease.

(A) TEM images obtained from 20- and 55 weeks-old *Tfam*^{fllox/fllox}**hNPHS2Cre* and littermate controls show normal foot process formation (representative pictures).

(B) TEM images obtained from 20- and 55 weeks-old *Tfam*^{fllox/fllox}**hNPHS2Cre* and littermate controls showing maintained mitochondrial morphology.

(C) Mitochondrial density in podocytes of *Tfam*^{fllox/fllox}**hNPHS2Cre* and littermate controls (based quantitative analysis of 48 TEM pictures obtained from 4 mice of each genotype, mean ± SD).

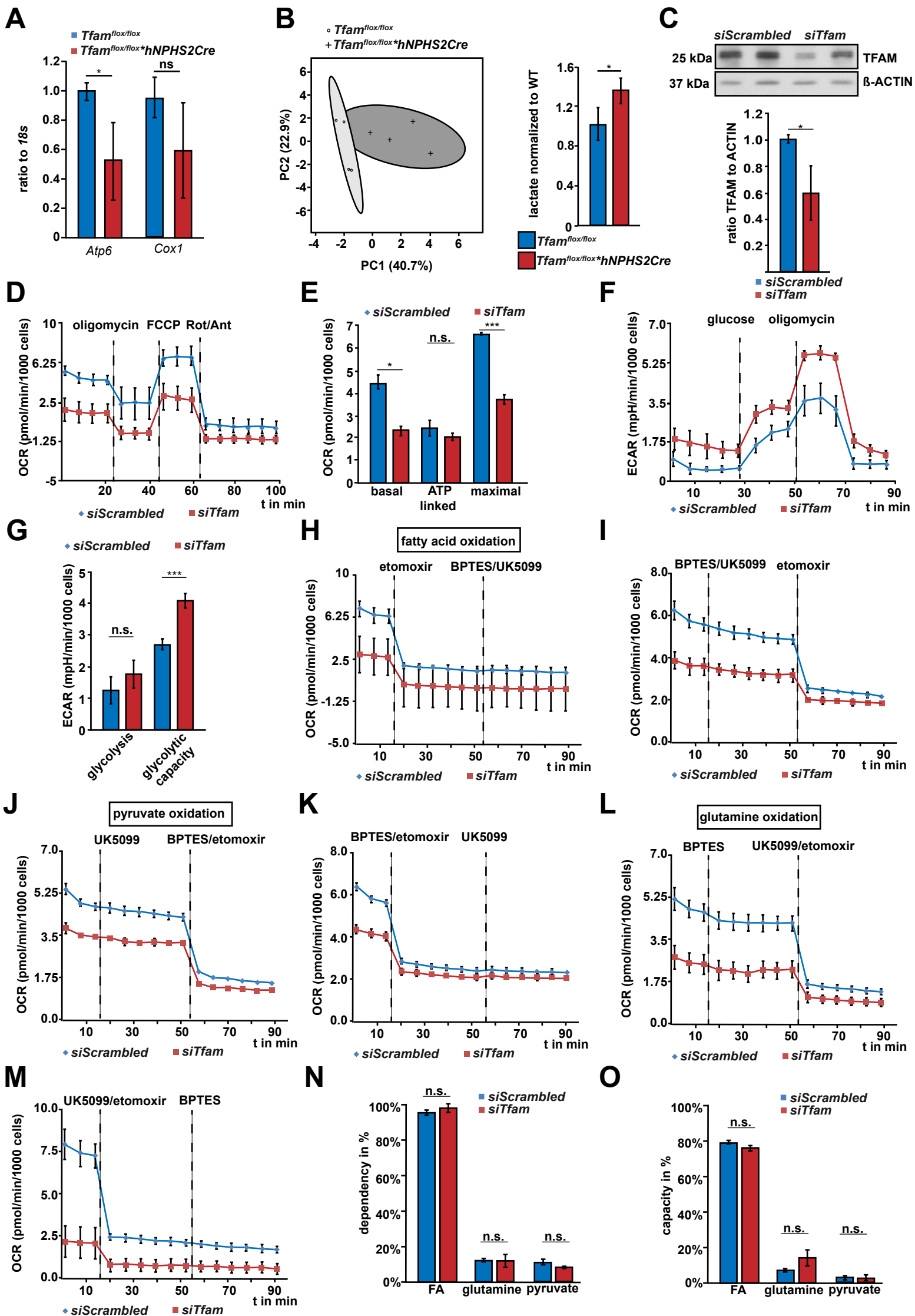


Figure S5: Impact of *Tfam* deletion on the expression of mitochondria encoded genes and function, Related to Figure 6

(A) qPCR for the abundance of mitochondrial DNA (Atp6, Cox I) normalized to genomic DNA (18s) (p-value * ≤ 0.05).

(B) Principal component analysis of metabolite abundance from kidney cortex obtained from 24-week-old mice of respective genotype assessed by unbiased GC-MS based metabolomic analysis (n=4 each group). Lactate levels normalized to WT (p-value * ≤ 0.05).

(C) Western blot and densitometry for the abundance of TFAM in human podocytes after siRNA-based knock-down compared to scrambled siRNA controls (p-value * ≤ 0.05).

(D) Mitochondrial function of human podocytes after knock-down of *Tfam* and respective controls. Oxygen consumption rate (OCR) was measured at basal level and after the sequential addition of oligomycin (1 mM), FCCP (0.5 mM), and rotenone (Rot; 1.0 mM) + antimycin A (Ant; 1.0 mM; n=3, technical replicates).

(E) Combined results underline the major role of *Tfam* for mitochondrial respiratory function as shown for basal respiration, ATP-linked oxygen consumption rate and maximal respiratory capacity (p-value * ≤ 0.05 and *** ≤ 0.001).

(F) Extracellular acidification rate (ECAR) of human podocytes with knock-down of *Tfam* and respective controls at baseline and after injection of glucose followed by oligomycin.

(G) Combined results underline the major impact of *Tfam* for anaerobic utilization of glucose as shown for glycolysis and maximal glycolytic capacity (p-value * ≤ 0.05 and *** ≤ 0.001).

(H) Dependency of fatty acid oxidation of human podocytes with knock-down for *Tfam* and respective controls obtained after etomoxir and BPTES/UK5099 injection. Final concentrations: etomoxir: 100 μM , BPTES: 30 μM , UK5099: 30 μM .

(I) Capacity of fatty acid oxidation of human podocytes with knock-down for *Tfam* and respective controls obtained after BPTES/UK5099 injection followed by etomoxir, Final concentrations: etomoxir: 100 μM , BPTES: 30 μM , UK5099: 30 μM .

(J) Dependency of pyruvate oxidation of human podocytes with knock-down for *Tfam* and respective controls obtained after UK5099 and BPTES/etomoxir injection. Final concentrations: UK5099: 30 μM , etomoxir: 100 μM , BPTES: 30 μM .

(K) Capacity of pyruvate oxidation of human podocytes with knock-down for *Tfam* and respective controls obtained after BPTES/etomoxir and UK5099 injection. Final concentrations: etomoxir: 100 μM , BPTES: 30 μM , UK5099: 30 μM .

(L) Dependency of glutamine oxidation of human podocytes with knock-down for *Tfam* and respective controls obtained after BPTES and UK5099/etomoxir injection. Final concentrations: BPTES: 30 μM , UK5099: 30 μM , etomoxir: 100 μM .

(M) Capacity of glutamine oxidation of human podocytes with knock-down for *Tfam* and respective controls obtained after UK5099/etomoxir and BPTES injection. Final concentrations: UK5099: 30 μM , etomoxir: 100 μM , BPTES: 30 μM .

(N) Statistics for substrate dependency of human podocytes with knock-down for *Tfam* and respective controls.

(O) Statistics for substrate capacity of human podocytes with knock-down for *Tfam* and respective controls.

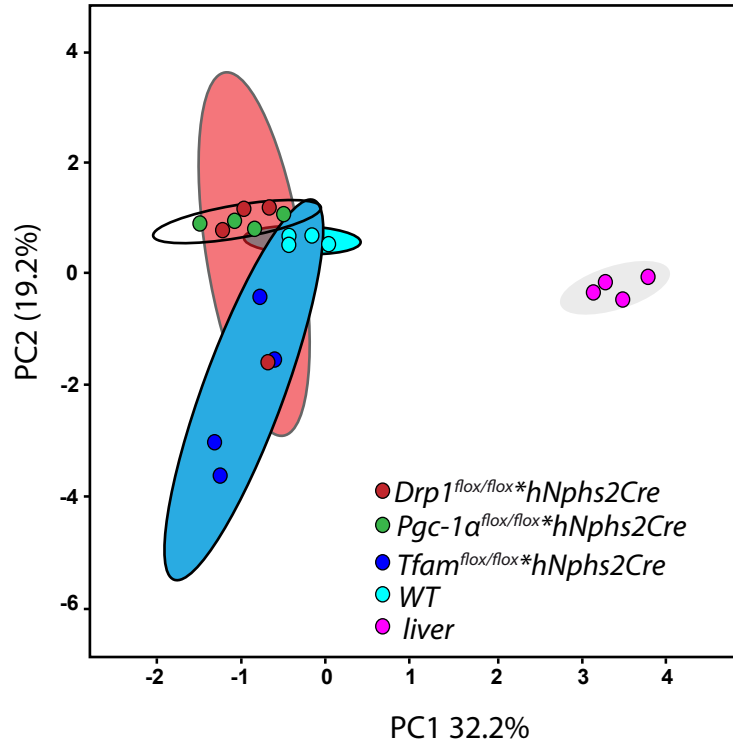
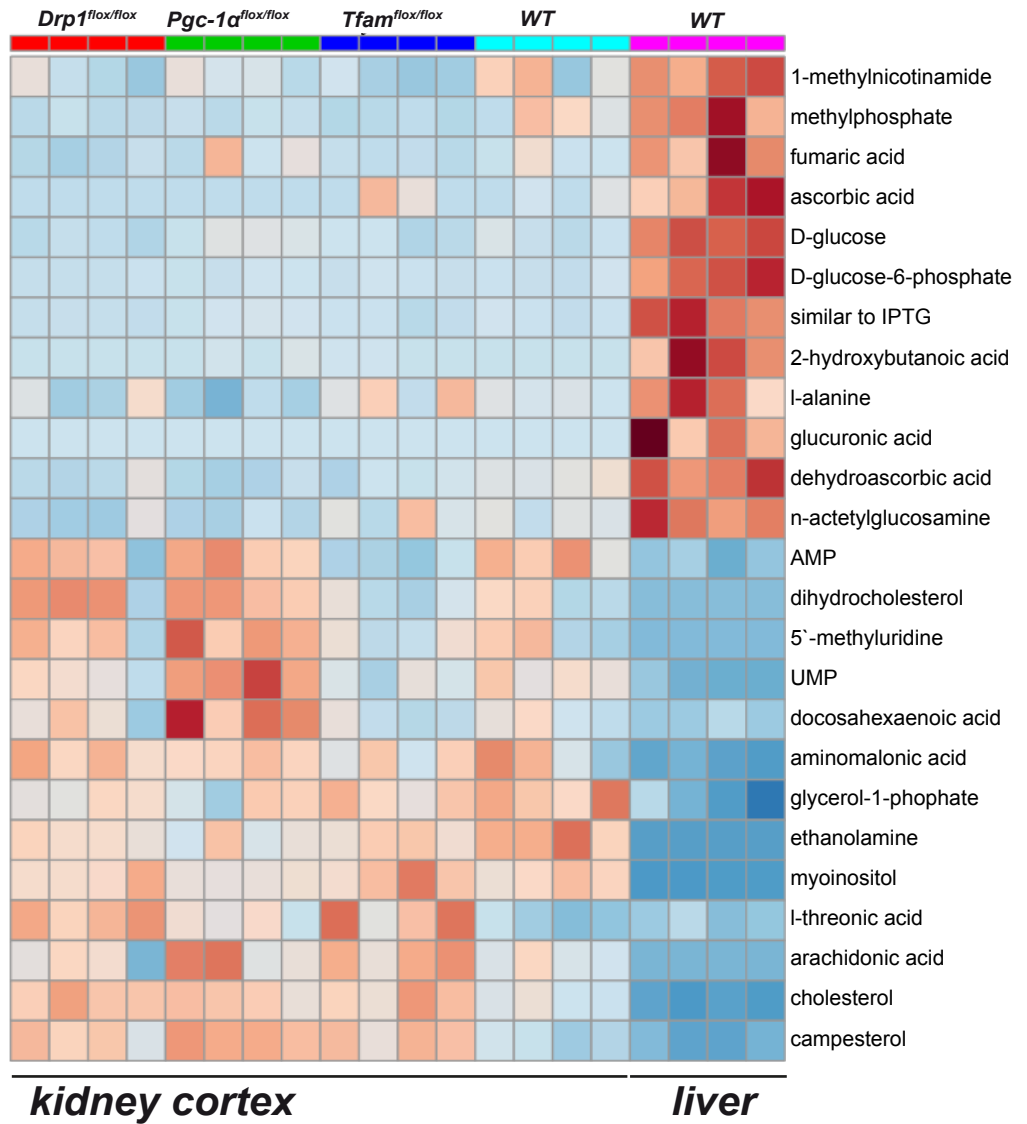
A**B**

Figure S6: Metabolic profiling of ex vivo isolated kidney cortex of *Drp1*, *Pgc-1 α* and *Tfam* mice, Related to Figure 7

(A) Principal component analysis of metabolites found in kidney cortex of respective genetic mouse models and liver tissue (n=4 each).

(B) Heat map of top 25 significantly different metabolites found in kidney cortex of respective genetic mouse models and liver tissue (n=4 each).